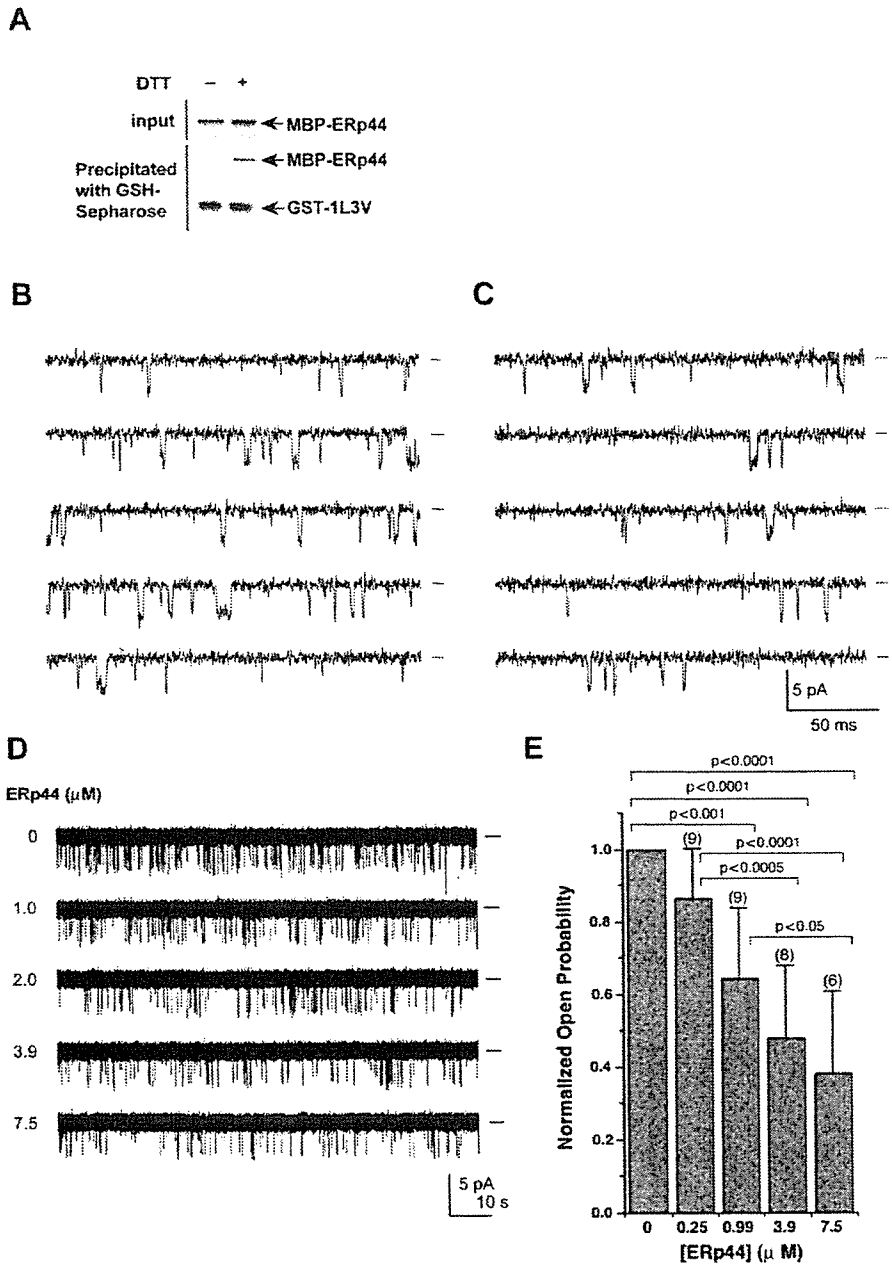

Figure 6. ERp44 Inhibits IP_3R1 in a Lipid Bilayer System

(A) MBP-ERp44 and GST-1L3V were incubated in the *trans* solution with (+) or without (–) 3 mM DTT and then precipitated with GSH-Sepharose. Precipitated proteins were analyzed by Western blotting.

(B and C) Sequential records before (B) and after addition (C) of 7.5 μM MBP-ERp44. Channels were recorded at −20 mV. Continuous 1 s records filtered at 1 kHz are shown.

(D) Effects of ERp44 on single-channel activity of IP_3R1 in the presence of 6.4 μM cytosolic (*cis*) IP_3 and 3 mM lumenal (*trans*) DTT. Serial additions of purified MBP-ERp44 were made to the lumenal compartment. Channel openings are shown as downward deflections from baseline (denoted by the horizontal lines). The data shown are representative of six independent experiments. Data were filtered at 0.5 kHz. The absolute values of open probability before the addition of ERp44 were in the 0.008–0.086 range.

(E) Dose-dependent inactivation of IP_3R1 by ERp44 under lumenal reducing conditions. The averages of open probabilities were normalized to the maximum IP_3R1 activity observed in each experiment. The data are means ± SD. Statistical analysis was done using repeated measures one-way ANOVA with Bonferoni's post-hoc tests. The number of independent trials is indicated above each bar.

respectively), indicating that ERp44 modulated the closed state of IP_3R1. Similarly, addition of ERp44 did not alter the amplitude of the single-channel current (3.7 ± 0.2 pA and 3.6 ± 0.2 pA [mean ± SD, n = 6] at −20 mV before versus after addition of MBP-ERp44, respectively). Raising the IP_3 concentration to 25 μM did not reverse the inhibitory effect of MBP-ERp44, and there was no indication that MBP-ERp44 lowers the IP_3 sensitivity of IP_3R1 (data not shown). No inactivation was observed in the absence of DTT (data not shown), further supporting the hypothesis that the free thiol group(s) in the L3V domain are involved in inhibition by ERp44. These bilayer studies revealed that ERp44 functions to maintain the closed state of IP_3R1 rather than affecting the characteristics of its open state.

Discussion

In this study we demonstrated that ERp44 directly interacts with the L3V domain of IP_3R1, thereby inhibiting its channel activity. This functional interaction is dependent on the pH, redox state, and $[Ca^{2+}]_{ER}$. It is particularly noteworthy that cysteine residues in the L3V domain of IP_3R1 play critical roles in both interaction with and inhibition by ERp44. This is the first example of a negative regulator of IP_3Rs on the ER lumen side and provides support for the hypothesis that IP_3Rs are specifically controlled by the intralumenal, in addition to by the cytosolic, environment.

Roles of Redox State, $[Ca^{2+}]_{ER}$, and pH in Dynamic Regulation of IP_3R by ERp44

It is widely accepted that the ER lumen is more oxidizing than the cytosol, and the ratio of reduced to oxidized glutathione in the ER lumen has been estimated to be from 3:1 to 1:1 (Hwang et al., 1992; Bass et al., 2003), suggesting that roughly 50%–75% of all lumenal cysteine residues are in the reduced (free thiol) form. However, it is also known that some proteins are either exclusively in the oxidized or the reduced state. While the mechanisms that control the redox state of extracellular proteins and ER oxidoreductases are being clarified (Sevier and Kaiser, 2002), how the redox state of other ER resident proteins (including IP_3Rs) is regulated is poorly understood. Our results indicate that the interaction between ERp44 and 1L3V weakens as the number of free thiol groups on 1L3V decreases (Figures 2D, 2F, and 5B). Therefore, if the cysteine residues of an IP_3R1 tetramer form a disulfide bond or are modified by, for example, nitrosylation, it would not bind to ERp44. Based on all of the evidence considered, we hypothesize that some of the cysteine residues in the L3V domain of IP_3R1 are in their free (reduced) form and that others have formed disulfide bonds or are modified. The disulfide bonds may be formed in the same polypeptide, between subunits, or with other molecules. IP_3R1 that have free cysteine residues in the L3V domain are subject to inhibition by ERp44. It must be pointed out that the number and approximate positions of cysteine residues are conserved in all IP_3R subtypes (Figure 1B), raising the possibility that forming a heterotetramer with these subtypes by disulfide bonds may be one way that the IP_3R1 polypeptide escapes inhibition. Whether the redox state, modification, or disulfide bond formation of these cysteine residues is controlled by a specific mechanism is a crucial and challenging question.

Previous studies have shown IICR to be diminished at low $[Ca^{2+}]_{ER}$, and this finding cannot be fully explained by the decreased Ca^{2+} concentration gradient across the ER membrane (e.g., Caroppo et al., 2003). Since the interaction between ERp44 and IP_3R1 is weaker when $[Ca^{2+}]_{ER}$ exceeds 100 μM (i.e., at resting levels, Figure 2E), it is tempting to speculate that the inhibition of IICR previously observed at low $[Ca^{2+}]_{ER}$ is due to enhanced binding of ERp44 to IP_3R1. More detailed investigation at both the cellular and the single-channel level is necessary to resolve this issue.

The pH in the ER lumen has been considered to be almost neutral and stable even during and after Ca^{2+} release (Foyouzi-Youssefi et al., 2000; Kim et al., 1998). However, it is also known that the pH in the lumen of the sarcoendoplasmic reticulum changes drastically after Ca^{2+} release (Kamp et al., 1998), and oligodendrocytes (glial cell type that have long and branched protrusions like neurons) have pH "microdomains," some of which could be below 6.5 (Ro and Carson, 2004). Thus, the pH in the ER lumen may also change in certain cell types or under certain conditions, and in such cases IP_3R1 may be more subject to inhibition by ERp44.

Physiological Significance of IP_3R1 Inhibition by ERp44

Central neurons express exclusively IP_3R1 (Taylor et al., 1999) and it is well known that localized Ca^{2+} release plays a variety of roles in these cell types (Berridge, 2002). In view of the fact that ERp44 can regulate IP_3R1 in a microenvironment-dependent manner, it is tempting to hypothesize that ERp44 is involved in the spatiotemporal regulation of localized Ca^{2+} release in neurons. Particularly, as both IICR and the redox state are involved in synaptic modulations (Inoue et al., 1998; Nishiyama et al., 2000; Knapp and Klann, 2002), ERp44 may also function in these processes. In addition, it was recently appreciated that some of the genetic abnormalities that cause neurodegenerative diseases augment IICR (Tang et al., 2003; Stutzmann et al., 2004), which may be the direct cause of neuronal death. Whether these IICR-activating mutations affect the function of ERp44, or even whether ERp44 can counteract them, are important pathological questions.

More generally, since the ER is the intersection of many signaling pathways (Berridge et al., 2003; Orrenius et al., 2003), inhibition of IP_3R1 by ERp44 may be involved in the feedback system by which information that has converged in the ER lumen is conveyed to the cytosol/nucleus in the form of $[Ca^{2+}]_C$. In other words, ERp44 translates the ER lumenal environment into a $[Ca^{2+}]_C$ by modulating IP_3R, and such a mechanism would allow the functions of the ER lumen (e.g., folding and glycosylation) and of the cytosol/nucleus (e.g., phosphorylation signaling and gene expression) to operate in a concerted matter.

Since the functions of many ER lumenal enzymes and chaperones are Ca^{2+} dependent, inhibition of Ca^{2+} release when the $[Ca^{2+}]_{ER}$ falls below the resting level would be consistent with maintaining their functions.

ERp44 was identified as a protein that forms mixed disulfide bonds with Ero1α, an ER oxidoreductase (Anelli et al., 2002), and it was shown to be involved in ER retention of Ero1α (Anelli et al., 2003). The functions of Ero1 family proteins are not fully understood, but since they play pivotal roles in oxidative protein folding (Tu and Weissman, 2002), ERp44 may play dual roles in protein folding: inhibiting Ca^{2+} release (which reinforces Ca^{2+}-dependent chaperones) by inactivating IP_3R1 and supporting disulfide bond formation by reinforcing the Ero1α/oxidoreductase system. The fact that ERp44 is induced during the unfolded protein responses (Anelli et al., 2002) fits well with this model.

Redox-Dependent Regulation of Cellular Ca^{2+} Signaling

It was very recently reported that SERCA 2b activity is modulated by CRT and ERp57, an ER lumenal oxidoreductase, in a $[Ca^{2+}]_{ER}$- and redox state-dependent manner (Li and Camacho, 2004). Since the pump activity of SERCA 2b is higher when thiol groups in its lumenal loop are reduced, when the ER lumenal environment shifts to the reducing condition, Ca^{2+} uptake by SERCA 2b should be enhanced (by ERp57) and Ca^{2+} release via IP_3R1 should be inhibited (by ERp44). In other words, SERCA 2b and IP_3R1 work together to increase $[Ca^{2+}]_{ER}$ under reducing conditions. This is reasonable since a reduced ER lumenal environment is unfavorable for protein folding and increasing $[Ca^{2+}]_{ER}$ benefits the function of the many chaperones and oxidoreductases that require a relatively high $[Ca^{2+}]_{ER}$. Finally, we obtained no indication that ERp57 (or PDI) associates with IP_3R1 (Supplemental Figure S6 online) or that ERp44 associates with SERCA 2b (data not shown).

Future Directions

To learn how ER lumenal conditions regulate the interaction between ERp44 and IP_3R1 and what the consequences of the interaction are in greater detail, it will be necessary to monitor ER lumenal conditions and the $[Ca^{2+}]_c$ in real time. It is also imperative to investigate the effect of ERp44 on IP_3R1 by using the planar lipid bilayer system under various conditions.

Finally, we were unable to find any protein in the brain (where IP_3R1 is exclusively expressed) that binds to the lumenal domain of IP_3R2 or IP_3R3, but these subtypes are likely to have different binding proteins that are not present in the brain. The fact that the cysteine residues in the L3V domain are conserved (Figure 1B) supports this hypothesis. Searching for such interacting protein(s), investigating how the lumenal environment regulates IP_3R2 and IP_3R3, and how it is related to ERp44/IP_3R1 are our next research challenges.

Experimental Procedures

Plasmids

Full-length ERp44 cDNA was obtained from P14 mouse cerebellum by the reverse transcriptase-polymerase chain reaction. The expression vectors for epitope-tagged or fluorescent protein-tagged ERp44, IP_3Rs, and their mutants were constructed by utilizing the polymerase chain reaction. The details of these methods, including the sequences of the primers used, will be supplied on request. All constructs were verified by DNA sequencing.

Antibodies

Rabbit polyclonal antibody to ERp44 was raised to purified His_6-ERp44 and affinity-purified with MBP-ERp44 coupled to CNBr-activated Sepharose 4B (Amersham). Other antibodies used were anti-IP_3R1 18A10, anti-IP_3R3 KM1082 (for both, see Hattori et al., 2004), anti-HA (12CA5, a gift of Dr. T. Yamamoto), anti-HA-Peroxidase (3F10, Roche), anti-CRT (Affinity BioReagents), anti-MBP (New England Biolabs), anti-human IgG (Vector Laboratories), anti-GST (Amersham), anti-GFP, and anti-actin (both Santa Cruz). The hybridoma producing anti-IgM (M-4 clone) was kindly provided by Dr. T. Kurosaki (Kansai Medical University).

Cell Culture and Transfection

COS-7, HeLa, and 293T cells were cultured in Dulbecco's modified Eagle medium supplemented with 10% heat-inactivated fetal bovine serum. DT40 cells were cultured in RPMI1640 medium supplemented with 10% heat-inactivated fetal bovine serum, 1% chicken serum, 100 U/ml penicillin and streptomycin, 2 mM glutamine, and 50 μM 2-mercaptoethanol. HeLa, COS-7, and 293T cells were transfected with expression vectors or siRNAs by means of TransIT (Mirus) or Lipofectamine2000 (Invitrogen). DT40 cells were transfected by electroporation with Nucleofector (Amaxa).

Identification of ERp44

1L3V-Fc or control Fc was expressed in 293T cells. After collecting the medium and incubating it with Protein-G Sepharose (Amersham) for 2 hr at 4°C, the beads were washed with 10 mM Tris-HCl (pH 8.0) and 150 mM NaCl. Approximately 0.2 mg of 1L3V-Fc or control Fc was coupled to beads, and the beads were loaded into a column. P14 mouse cerebella were washed with ice-cold PBS and homogenized in a buffer containing 0.32 M sucrose, 10 mM Tris-HCl (pH 7.5), 2 mM EDTA, and 1 mM DTT. The homogenates were centrifuged for 1 hr at 100,000 × *g* at 2°C, and after solubilizing the pellet in buffer containing 30 mM sodium acetate, 150 mM NaCl, 4 mM $CaCl_2$, and 1% Triton X-100, the solution was centrifuged at 10,000 × *g* for 15 min. The supernatant was applied to affinity columns, and the columns were washed with the same buffer, followed by neutral Ca^{2+} buffer (10 mM Tris-HCl [pH 8.0], 150 mM NaCl, 4 mM $CaCl_2$, and 1% Triton X-100), and finally neutral chelator buffer (10 mM Tris-HCl [pH 8.0], 150 mM NaCl, 5 mM EDTA, 5 mM EGTA, and 1% Triton X-100).

Western Blot Analysis

Proteins were resolved by SDS-PAGE and transferred to a polyvinylidene difluoride membrane. The membranes were blocked with 5% skim milk in PBS containing 0.05% Tween-20 (PBST) for 30 min and probed with the primary antibody for 3 hr at room temperature (RT). After washing with PBST, the membranes were incubated with a suitable secondary antibody and signals were detected with an ECL Plus kit (Amersham).

IP and GST-Pulldown Assay

For IP, cells were washed with PBS and then exposed to 2 mM DSP (Pierce) in PBS for 30 min at RT. After washing with PBS, the cells were solubilized in TNE buffer (150 mM Tris-HCl [pH 7.5], 500 mM NaCl, 1 mM EDTA, 1% Triton X-100, 0.1% SDS), and the lysates were incubated with the antibodies indicated and Protein-G Sepharose for 2 hr at 4°C. The beads were then washed five times with TNE buffer, and the proteins were eluted by boiling in SDS-PAGE sampling buffer.

Recombinant proteins were expressed in *E. coli* BL21 and purified with GSH-Sepharose (Amersham) or Amylose Resin (New England Biolabs). GST or GST fusion proteins were incubated with MBP or MBP fusion proteins for 1 hr at 4°C in acidic solution (30 mM NaOAc [pH 5.2], 150 mM NaCl, 4 mM $CaCl_2$, 0.1% Triton X-100). ERp44 and GST fusion proteins were incubated in neutral buffer (20 mM Tris-HCl [pH 7.5], 150 mM NaCl, 5 mM EGTA, 0.1% Triton X-100) with or without 3 mM DTT. GST-1L3V and MBP-ERp44 were incubated in neutral buffer or neutral buffer in which EGTA had been replaced with $CaCl_2$. The experiments in Figures 2D, 2E, 2J, and 2K were carried out in neutral buffer containing 3 mM DTT.

RNA Interference

SiRNA duplexes were purchased from Dharmacon. The target sequences were siControl-C (5′-AAGUAGUGUAUGCUAGAGUGG-3′), siERp44-C (5′-AAGUAGUGUUUGCCAGAGUUG-3′), siControl-3U (5′-AACAGCACCAUCGACCAACGU-3′), siERp44-3U (5′-AACAGCAGCAUCAACCUACGU-3′).

Ca^{2+} Imaging

At 24–48 hr following transfection, cells were incubated for 30 min with 5 μM fura-2 AM (Dojindo). The cells were then placed on the stage of an inverted microscope (IX-70; Olympus, Japan) and perfused with balanced salt solution (BSS). Image capture and processing were performed with an Argus 50/CA system (Hamamatsu Photonics, Japan) at RT by a standard ratiometric method (excited at 340 nm and 380 nm). Fluorescence images of GFP and RFP were acquired separately and saved in the computer in the same optical fields as the fluorescence images for Ca^{2+} imaging. We also performed Ca^{2+}-imaging experiments using fura-4F AM in all cell types used in this study and confirmed that all of the responses obtained in experiments using fura-2 were not saturated (data not shown).

Planar Lipid Bilayer Experiments

Single-channel recordings of IP_3R1 in mouse cerebellar microsomes were performed as described previously (Michikawa et al., 1999), with some modifications. The *cis* chamber contained 108 mM Tris dissolved in 250 mM HEPES (pH 7.33), 1.11 mM K_2-H-HEDTA (N-hydroxyethylethylenediamine-N,N′,N′-triacetic acid), 0.12 mM K-Ca-HEDTA. The *trans* chamber contained 250 mM HEPES (pH 7.33), 53 mM $Ba(OH)_2$, 3 mM DTT. IP_3R1 was activated by the addition of 6.4 μM IP_3 and 0.5 mM ATP to the *cis* chamber. Purified MBP or MBP-ERp44 was added directly to the *trans* side. The currents were amplified (Axon Instruments), filtered at 1 kHz with a low-pass Bessel filter (NF Instruments), and sampled at 10 kHz. Single-channel data were analyzed as described previously (Michikawa et al., 1999).

Acknowledgments

We thank K. Nakamura and A. Suzuki for excellent technical assistance and Dr. T. Inoue for invaluable discussions and technical help. We also thank Drs. A. Miyawaki, H. Bito, T. Shimizu, and A. Mizutani for critical reading of the manuscript. This study was supported by the grant from the JST, and the Grants-in-Aid (M.H. and K.M.) and The 21st Century COE Program, Center for Integrated Brain Medical Science, from the Ministry of Education, Culture, Sports, Science and Technology, Japan.

Received: April 28, 2004
Revised: August 24, 2004
Accepted: November 18, 2004
Published: January 13, 2005

References

Anelli, T., Alessio, M., Mezghrani, A., Simmen, T., Talamo, F., Bachi, A., and Sitia, R. (2002). ERp44, a novel endoplasmic reticulum folding assistant of the thioredoxin family. EMBO J. *21*, 835–844.

Anelli, T., Alessio, M., Bachi, A., Bergamelli, L., Bertoli, G., Camerini, S., Mezghrani, A., Ruffato, E., Simmen, T., and Sitia, R. (2003). Thiol-mediated protein retention in the endoplasmic reticulum: the role of ERp44. EMBO J. *22*, 5015–5022.

Bass, R., Ruddock, L.W., Klappa, P., and Freedman, R.B. (2003). A major fraction of ER-located glutathione is present as mixed disulfides with protein. J. Biol. Chem. *279*, 5257–5262.

Berridge, M.J. (2002). Neuronal calcium signaling. Neuron *21*, 13–26.

Berridge, M.J., Bootman, M.D., and Roderick, H.L. (2003). Calcium signalling: dynamics, homeostasis and remodelling. Nat. Rev. Mol. Cell Biol. *4*, 517–529.

Boehning, D., and Joseph, S.K. (2000). Functional properties of recombinant type I and type III inositol 1, 4,5-trisphosphate receptor isoforms expressed in COS-7 cells. J. Biol. Chem. *275*, 21492–21499.

Camacho, P., and Lechleiter, J.D. (1995). Calreticulin inhibits repetitive intracellular Ca^{2+} waves. Cell *82*, 765–771.

Caroppo, R., Colella, M., Colasuonno, A., DeLuisi, A., Debellis, L., Curci, S., and Hofer, A.M. (2003). A reassessment of the effects of luminal $[Ca^{2+}]$ on inositol 1,4,5-trisphosphate-induced Ca^{2+} release from internal stores. J. Biol. Chem. *278*, 39503–39508.

Choe, C.U., Harrison, K.D., Grant, W., and Ehrlich, B.E. (2004). Functional coupling of chromogranin with inositol 1,4,5-trisphosphate receptor shapes calcium signaling. J. Biol. Chem. *279*, 35551–35556.

Foyouzi-Youssefi, R., Arnaudeau, S., Borner, C., Kelley, W.L., Tschopp, J., Lew, D.P., Demaurex, N., and Krause, K.H. (2000). Bcl-2 decreases the free Ca^{2+} concentration within the endoplasmic reticulum. Proc. Natl. Acad. Sci. USA *97*, 5723–5728.

Hattori, M., Suzuki, A.Z., Higo, T., Miyauchi, H., Michikawa, T., Nakamura, T., Inoue, T., and Mikoshiba, K. (2004). Distinct roles of inositol 1,4,5 trisphosphate receptor types 1 and 3. J. Biol. Chem. *279*, 11967–11975.

Hwang, C., Sinskey, A.J., and Lodish, H.F. (1992). Oxidized redox state of glutathione in the endoplasmic reticulum. Science *257*, 1496–1502.

Inoue, T., Kato, K., Kohda, K., and Mikoshiba, K. (1998). Type 1 inositol 1,4,5-trisphosphate receptor is required for induction of long-term depression in cerebellar Purkinje neurons. J. Neurosci. *18*, 5366–5373.

Kamp, F., Donoso, P., and Hidalgo, C. (1998). Changes in luminal pH caused by calcium release in sarcoplasmic reticulum vesicles. Biophys. J. *74*, 290–296.

Kim, J.H., Johannes, L., Goud, B., Antony, C., Lingwood, C.A., Daneman, R., and Grinstein, S. (1998). Noninvasive measurement of the pH of the endoplasmic reticulum at rest and during calcium release. Proc. Natl. Acad. Sci. USA *95*, 2997–3002.

Knapp, L.T., and Klann, E. (2002). Role of reactive oxygen species in hippocampal long-term potentiation: contributory or inhibitory? J. Neurosci. Res. *70*, 1–7.

Li, Y., and Camacho, P. (2004). Ca^{2+}-dependent redox modulation of SERCA 2b by ERp57. J. Cell Biol. *164*, 35–46.

Mattson, M.P. (2004). Pathways towards and away from Alzheimer's disease. Nature *430*, 631–639.

Meldolesi, J., and Pozzan, T. (1998). The endoplasmic reticulum Ca^{2+} store: a view from the lumen. Trends Biochem. Sci. *23*, 10–14.

Michikawa, T., Hirota, J., Kawano, S., Hiraoka, M., Yamada, M., Furuichi, T., and Mikoshiba, K. (1999). Calmodulin mediates calcium-dependent inactivation of the cerebellar type 1 inositol 1,4,5-trisphosphate receptor. Neuron *23*, 799–808.

Nishiyama, M., Hong, K., Mikoshiba, K., Poo, M.M., and Kato, K. (2000). Calcium stores regulate the polarity and input specificity of synaptic modification. Nature *408*, 584–588.

Orrenius, S., Zhivotovsky, B., and Nicotera, P. (2003). Regulation of cell death: the calcium-apoptosis link. Nat. Rev. Mol. Cell Biol. *4*, 552–565.

Paschen, W. (2003). Mechanisms of neuronal cell death: diverse roles of calcium in the various subcellular compartments. Cell Calcium *34*, 305–310.

Patterson, R.L., Boehning, D., and Snyder, S.H. (2004). Inositol 1,4,5-trisphosphate receptors as signal integrators. Annu. Rev. Biochem. *73*, 437–465.

Ro, H.A., and Carson, J.H. (2004). pH microdomains in oligodendrocytes. J. Biol. Chem. *279*, 37115–37123.

Roderick, L.H., Llewellyn, D.H., Campbell, A.K., and Kendall, J.M. (1998). Role of calreticulin in regulating intracellular Ca^{2+} storage and capacitative Ca^{2+} entry in HeLa cells. Cell Calcium *24*, 253–262.

Sevier, C.S., and Kaiser, C.A. (2002). Formation and transfer of disulphide bonds in living cells. Nat. Rev. Mol. Cell Biol. *3*, 836–847.

Stutzmann, G.E., Caccamo, A., LaFerla, F.M., and Parker, I. (2004). Dysregulated IP_3 signaling in cortical neurons of knock-in mice expressing an Alzheimer's-linked mutation in presenilin1 results in exaggerated Ca^{2+} signals and altered membrane excitability. J. Neurosci. *24*, 508–513.

Sugawara, H., Kurosaki, M., Takata, M., and Kurosaki, T. (1997). Genetic evidence for involvement of type 1, type 2 and type 3 inositol

1,4,5-trisphosphate receptors in signal transduction through the B-cell antigen receptor. EMBO J. *16*, 3078–3088.

Takei, K., Shin, R.M., Inoue, T., Kato, K., and Mikoshiba, K. (1998). Regulation of nerve growth mediated by inositol 1,4,5-trisphosphate receptors in growth cones. Science *282*, 1705–1708.

Tang, T.S., Tu, H., Chan, E.Y., Maximov, A., Wang, Z., Wellington, C.L., Hayden, M.R., and Bezprozvanny, I. (2003). Huntingtin and huntingtin-associated protein 1 influence neuronal calcium signaling mediated by inositol-(1,4,5) trisphosphate receptor type 1. Neuron *39*, 227–239.

Taylor, C.W., Genazzani, A.A., and Morris, S.A. (1999). Expression of inositol trisphosphate receptors. Cell Calcium *26*, 237–251.

Thrower, E.C., Choe, C.U., So, S.H., Jeon, S.H., Ehrlich, B.E., Yoo, S.H. (2003). A functional interaction between chromogranin B and the inositol 1,4,5-trisphosphate receptor/Ca^{2+} channel. J. Biol. Chem. *278*, 49699–49706.

Tu, B.P., and Weissman, J.S. (2002). The FAD- and O_2-dependent reaction cycle of Ero1-mediated oxidative protein folding in the endoplasmic reticulum. Mol. Cell *10*, 983–994.

Xiang, Y., Li, Y., Zhang, Z., Cui, K., Wang, S., Yuan, X.B., Wu, C.P., Poo, M.M., and Duan, S. (2002). Nerve growth cone guidance mediated by G protein-coupled receptors. Nat. Neurosci. *5*, 843–848.

The EMBO Journal (2004) 23, 1977–1986 | © 2004 European Molecular Biology Organization | All Rights Reserved 0261-4189/04
www.embojournal.org

THE EMBO JOURNAL

A novel protein-conjugating system for Ufm1, a ubiquitin-fold modifier

Masaaki Komatsu[1], Tomoki Chiba[1], Kanako Tatsumi[1], Shun-ichiro Iemura[2], Isei Tanida[3], Noriko Okazaki[4], Takashi Ueno[3], Eiki Kominami[3], Tohru Natsume[2] and Keiji Tanaka[1,*]

[1]Department of Molecular Oncology, Tokyo Metropolitan Institute of Medical Science, Bunkyo-ku, Tokyo, Japan, [2]National Institutes of Advanced Industrial Science and Technology, Biological Information Research Center (JBIRC), Kohtoh-ku, Tokyo, Japan, [3]Department of Biochemistry, Juntendo University School of Medicine, Bunkyo-ku, Tokyo, Japan and [4]Kazusa DNA Research Institute, Kazusa-Kamatari, Kisarazu, Chiba, Japan

Several studies have addressed the importance of various ubiquitin-like (UBL) post-translational modifiers. These UBLs are covalently linked to most, if not all, target protein(s) through an enzymatic cascade analogous to ubiquitylation, consisting of E1 (activating), E2 (conjugating), and E3 (ligating) enzymes. In this report, we describe the identification of a novel ubiquitin-fold modifier 1 (Ufm1) with a molecular mass of 9.1 kDa, displaying apparently similar tertiary structure, although lacking obvious sequence identity, to ubiquitin. Ufm1 is first cleaved at the C-terminus to expose its conserved Gly residue. This Gly residue is essential for its subsequent conjugating reactions. The C-terminally processed Ufm1 is activated by a novel E1-like enzyme, Uba5, by forming a high-energy thioester bond. Activated Ufm1 is then transferred to its cognate E2-like enzyme, Ufc1, in a similar thioester linkage. Ufm1 forms several complexes in HEK293 cells and mouse tissues, revealing that it conjugates to the target proteins. Ufm1, Uba5, and Ufc1 are all conserved in metazoa and plants but not in yeast, suggesting its potential roles in various multicellular organisms.
The EMBO Journal (2004) **23**, 1977–1986. doi:10.1038/sj.emboj.7600205; Published online 8 April 2004
Subject Categories: proteins
Keywords: Uba5; ubiquitin; ubiquitin fold; ubiquitin-like protein; Ufm1

Introduction

Protein modification plays a pivotal role in the regulation and expansion of genetic information. In the past two decades, a new type of post-translational protein-modifying system has been identified whose uniqueness is that protein(s) is used as a ligand, that is, modification of protein, by protein, and for protein. A typical system is the ubiquitylation, a modification system in which a single or multiple ubiquitin molecules are attached to a protein, which serves as a signaling player that controls a variety of cellular functions (Hershko and Ciechanover, 1998; Pickart, 2001). Protein ubiquitylation is catalyzed by an elaborate system highly regulated in the cells, which is catalyzed by a sequential reaction of multiple enzymes consisting of activating (E1), conjugating (E2), and ligating (E3) enzymes. E1, which initiates the reaction, forms a high-energy thiolester bond with ubiquitin via adenylation in an ATP-dependent manner. The E1-activated ubiquitin is then transferred to E2 in a thioester linkage. In some cases, E2 can directly transfer the ubiquitin to substrate proteins in an isopeptide linkage; however, E2s mostly requires the participation of E3 to achieve substrate-specific ubiquitylation reaction in the cells. E3s are defined as enzymes required for recognition of specific substrates for ubiquitylation, other than E1 and E2 (Varshavsky, 1997; Bonifacino and Weissman, 1998; Glickman and Ciechanover, 2002).

A set of novel molecules called ubiquitin-like proteins (UBLs) that have structural similarities to ubiquitin has been recently identified (Jentsch and Pyrowolakis, 2000). They are divided into two subclasses: type-1 UBLs, which ligate to target proteins in a manner similar, but not identical, to the ubiquitylation pathway, such as SUMO, NEDD8, and UCRP/ISG15, and type-2 UBLs (also called UDPs, ubiquitin-domain proteins), which contain ubiquitin-like structure embedded in a variety of different classes of large proteins with apparently distinct functions, such as Rad23, Elongin B, Scythe, Parkin, and HOIL-1 (Tanaka *et al*, 1998; Jentsch and Pyrowolakis, 2000; Yeh *et al*, 2000; Schwartz and Hochstrasser, 2003).

In this report, we describe a unique human UBL-type modifier named ubiquitin-fold modifier 1 (Ufm1) that is synthesized in a precursor form consisting of 85 amino-acid residues. We also identified the human activating (Uba5) and conjugating (Ufc1) enzymes for Ufm1. Prior to activation by Uba5, the extra two amino acids at the C-terminal region of the human proUfm1 protein are removed to expose Gly whose residue is necessary for conjugation to target molecule(s). Lastly, we show that the mature Ufm1 is conjugated to yet unidentified endogenous proteins, forming ~28, 38, 47, and 70 kDa complexes in human HEK293 cells and various mouse tissues.

Results

Identification of a novel protein-activating enzyme, Uba5

Our initial plan was to identify the molecule(s) that interacts with human Atg8p homolog GATE16, a type-1 UBL modifier required for autophagy (Klionsky and Emr, 2000; Ohsumi, 2001), using a yeast two-hybrid screening. Please note that the nomenclature of the autophagy-related genes was recently unified as *ATG* (Klionsky *et al*, 2003). Among several

*Corresponding author. Department of Molecular Oncology, The Tokyo Metropolitan Institute of Medical Science, 3-18-22 Honkomagome, Bunkyo-ku, Tokyo 113-8613, Japan. Tel.: +81 3 3823 2237; Fax: +81 3 3823 2237; E-mail: tanakak@rinshoken.or.jp

Received: 1 December 2003; accepted: 15 March 2004; published online; 8 April 2004

positive clones, we identified fragments of FLJ23251 (Figure 1A), which encodes a 404-amino-acid protein highly conserved in various multicellular organisms, such as *Homo sapiens*, *Caenorhabditis elegans*, *Drosophila melanogaster*, and *Arabidopsis thaliana*, but absent in yeasts (*Saccharomyces cerevisiae* and *Schizosaccharomyces pombe*) (Figure 1B). The sequence of FLJ23251 in the region containing residues 72–229 is highly homologous to the corresponding regions in Uba1 (i.e., E1 for ubiquitin) and other E1-like proteins for UBLs including the ATP-binding motif (GXGXXG) (Figure 1A and B). We named this protein Uba5, because it is a member of the E1-like enzyme family. Uba5 also has a metal-binding motif conserved in other E1-like enzymes such as Uba2, Uba3, Uba4, and Atg7. Most of E1-like enzymes have an active site Cys residue within the conserved 10–20 amino-acid residues downstream from the metal-binding

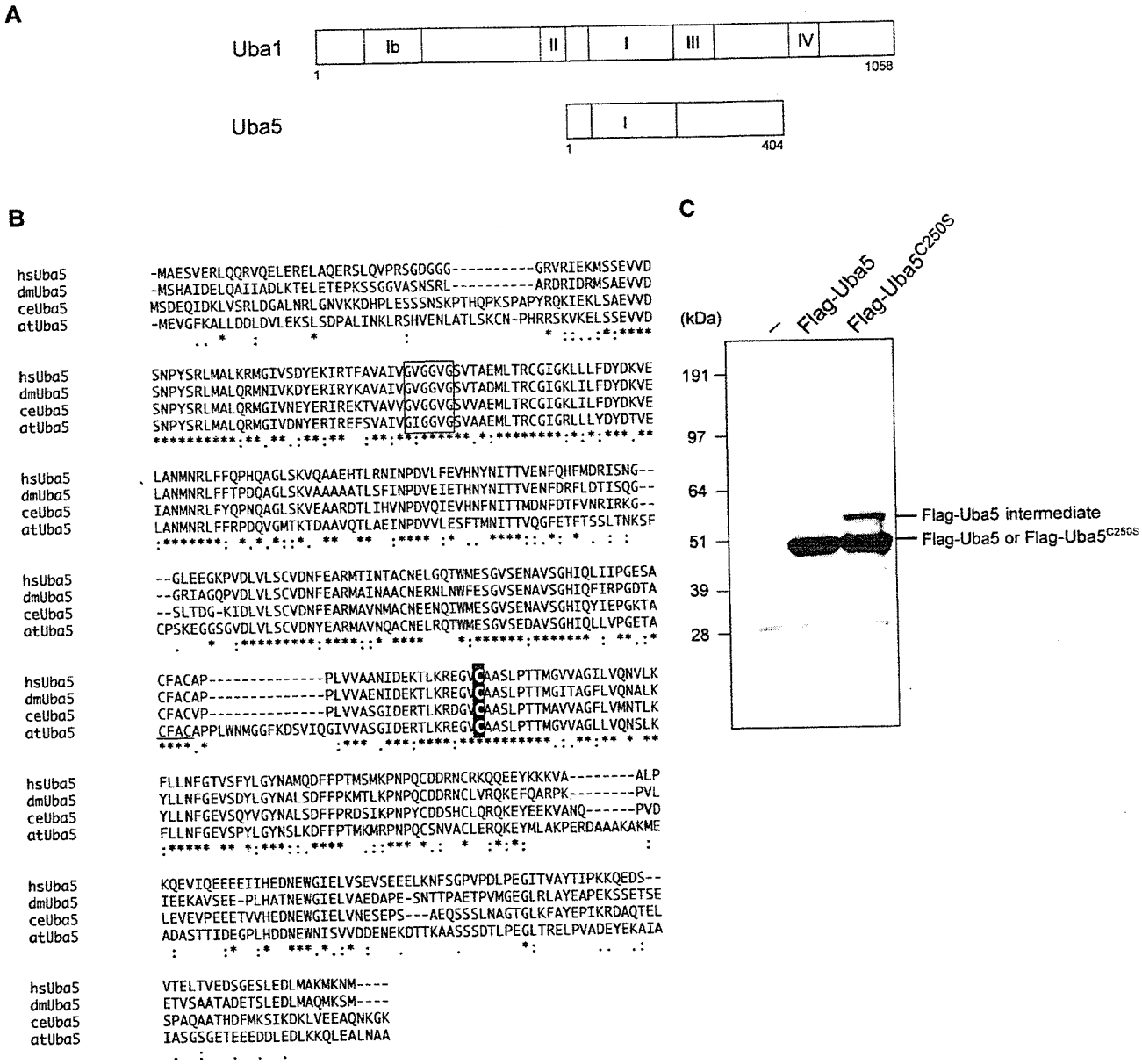

Figure 1 Uba5, a novel E1-like enzyme. (**A**) Schematic representation of Uba1 and Uba5 in *H. sapiens*. Uba1 is divided into several domains, including I, Ib, II, III, and IV boxes, which are conserved in other E1-like enzymes, and other regions without obvious similarity, described previously (Komatsu *et al*, 2001). Note that Uba5 is of a relatively small size and includes the box I and two other parts. The box I region of Uba1 (amino acids 459–611) has 48.4% similarity and 22.3% identity to amino acids 72–229 of Uba5, which includes the conserved ATP-binding motif (GXGXXG). The sequence of Uba5 is available from GenBank™ under the accession number AK026904. hs, *H. sapiens*; ce, *C. elegans*; dm, *D. melanogaster*; at, *A. thaliana*. (**B**) Sequence alignment of hsUba5 and its homologs of other species (dm, NM_132494; ce, NM_058847; at, NM_100414). The amino-acid sequence of hsUba5 is compared by the ClustalW program. *Asterisks*, identical amino acids; *single* and *double dots*, weakly and strongly similar amino acids, respectively, determined by the criteria of ClustalW program. *Open box* indicates an ATP-binding motif. The putative active site Cys residue is boxed in black. The metal-binding motif is underlined. (**C**) Identification of the intermediate linked to Uba5 in HEK293 cells. Both Uba5 and Uba5^{C250S}, in which the predicted active site Cys positioned at 250 was changed to Ser by site-directed mutagenesis, were tagged with Flag peptide at N-terminus, resulting in Flag-Uba5 and Flag-Uba5^{C250S}, respectively. Each Flag-Uba5 and Flag-Uba5^{C250S} was expressed in HEK293 cells. The cell lysates were subjected to SDS–PAGE and analyzed by immunoblotting with anti-Flag antibody.

motif. In the case of Uba5, the Cys^{250} seems to be the most possible active site Cys residue (Figure 1B). If an active site Cys residue within an E1 and E1-like enzymes is changed to Ser, an O-ester bond instead of a thioester bond is formed with its respective modifier protein and the intermediates become stable even under reducing conditions. Therefore, we mutated Cys^{250} within Uba5 to Ser and expressed it as a Flag-fused $Uba5^{C250S}$ (Flag-$Uba5^{C250S}$) or Flag-Uba5 as control in HEK293 cells. As shown in Figure 1C, both Flag-Uba5 and Flag-$Uba5^{C250S}$ were expressed as ~50 kDa proteins in HEK293 cells. When Flag-$Uba5^{C250S}$ was expressed, an additional band with a higher molecular mass of ~60 kDa was clearly observed, indicating that Flag-$Uba5^{C250S}$ forms an intermediate complex with an endogenous protein. These results suggest that Uba5 is indeed a novel protein-activating enzyme for a presumptive modifier (see below).

Identification of a novel ubiquitin-fold molecule, Ufm1

Because Uba5 was identified as GATE-16-binding protein, we initially assumed that Uba5 is another GATE-16-activating enzyme, in addition to Atg7. To test this possibility, we examined whether $Uba5^{C250S}$ (the presumptive active site Cys at position 250 was replaced by Ser) forms an intermediate complex with GATE-16 or not. Unexpectedly, we could not identify a stable complex between $Uba5^{C250S}$ and GATE-16 (data not shown). Therefore, we attempted to identify a protein(s) that physically associates with Uba5 in the cells. To do this, Flag-Uba5 was expressed in HEK293 cells, then immunoprecipitated by anti-Flag antibody. The immunoprecipitates were eluted with a Flag peptide, then digested with Lys-C endopeptides (*Achromobacter* protease I) and the cleaved fragments were directly analyzed using a highly sensitive 'direct nano-flow LC–MS/MS' system as described in Materials and methods. Following database search, a total of 28 peptides were assigned to MS/MS spectra obtained from four nano-LC–MS/MS analyses for the Flag-Uba5-associated complexes. These peptide data identified three proteins as Uba5-associated components: GATE-16, and hypothetical proteins BM-002 and CGI-126 (excluding the bait protein Uba5 and the background proteins, such as HSP70 and keratins).

One of these identified proteins, BM-002, is an 85-amino-acid protein with a predicted molecular mass of ~9.1 kDa. This protein is conserved in multicellular organisms, but not in yeasts, like Uba5 (Figure 2A). The human BM-002 has high identity over the species in the central region but has elongated sequences at both N- and C-terminal regions in some species. Although the protein shows no clear overall sequence identity to ubiquitin or other modifiers (Figure 2B), the tertiary structure of BM-002 displays a striking resemblance to human ubiquitin (Figure 2C). The human structure of BM-002 was constructed by a computer-assisted modeling, based on the structure of its *C. elegans* homolog that has been analyzed previously, as a protein possessing 'ubiquitin-like fold' with secondary structure elements ordered β–β–α–β–β–α (α-helix and β-sheet) along the sequence (Cort *et al*, 2002). Thus, we named human BM-002 as Ufm1.

Ubiquitin is synthesized in a precursor form that must be processed by de-ubiquitylating enzymes (DUBs) to generate a Gly–Gly sequence at the C-terminus. Similarly, Ufm1 has a single Gly residue conserved across species at the C-terminal region, although the length and sequences of amino acids extending from this Gly residue vary among species. To test whether the C-terminus of Ufm1 is post-translationally cleaved, we constructed an expression vector for Ufm1 tagged at both the N- and C-ends, that is, a Flag epitope at the N-terminus and an HA epitope at the C-terminus (Flag-Ufm1-HA) (Figure 2D). After transfection of Flag-Ufm1-HA into HEK293 cells, the cell lysate was subjected to SDS–PAGE, and Flag-Ufm1-HA was detected by immunoblotting. A 10-kDa protein corresponding to Ufm1 was recognized with anti-Flag antibody, while no appreciable protein was observed with anti-HA antibody (Figure 2E, lanes 2 and 7). The mobility on SDS–PAGE was similar to that of Flag-Ufm1ΔC2 (equivalent to mature $Ufm1^{1-83}$ protein) lacking the C-terminal Ser^{84} and Cys^{85} of proUfm1 (Figure 2E, lane 4). These results suggested that the C-terminus of Ufm1 is post-translationally cleaved in the cells, producing mature Ufm1 with the C-terminal Gly^{83} residue. It is known that the replacement of C-terminal Gly residue of Ub and other UBLs with an Ala residue inhibits the C-terminal processing (Kabeya *et al*, 2000; Tanida *et al*, 2003). To examine whether Gly^{83} of Ufm1 is essential for the cleavage, Gly^{83} of Flag-Ufm1-HA was mutated to Ala, and expressed in HEK293 cells (Figure 2D, Flag-$Ufm1^{G83A}$-HA). The mobility of most Flag-$Ufm1^{G83A}$-HA on SDS–PAGE was apparently slower than that of Flag-Ufm1-HA (Figure 2E, lane 3). This mutant was recognized by immunoblotting with anti-HA antibody as well as anti-Flag antibody, suggesting that mutation Gly^{83} to Ala confers resistance to its C-terminal cleavage.

Uba5 is an Ufm1-activating enzyme

We next investigated whether Uba5 forms an intermediate complex with Ufm1. We expressed Flag-Uba5 or Flag-$Uba5^{C250S}$ with Myc-tagged Ufm1 (Myc-Ufm1) in HEK293 cells. Myc-tagged Ufm1ΔC3 lacking the C-terminal Gly^{83} of mature Ufm1 (Myc-Ufm1ΔC3; i.e., deletion form of three residues from precursor $Ufm1^{1-85}$ protein) was used as control. Each cell lysate was prepared and analyzed by immunoblotting with anti-Flag antibody. Flag-$Uba5^{C250S}$ formed an intermediate with an endogenous protein as shown in Figure 1 (Figure 3A, lane 7). When Flag-$Uba5^{C250S}$ was coexpressed with Myc-Ufm1, the intermediate shifted to higher molecular weight (Figure 3A, lane 8). The higher band was not detected when Myc-Ufm1ΔC3 was coexpressed (Figure 3A, lane 9). To verify that the intermediate is indeed the Uba5–Ufm1 complex, Flag-$Uba5^{C250S}$ was immunoprecipitated and blotted with anti-Flag and anti-Myc antibody. Consistent with the above data, a higher sized intermediate was observed when Flag-$Uba5^{C250S}$ was coexpressed with Myc-Ufm1 (Figure 3B, top panel, lane 5), but not alone or with Myc-Ufm1ΔC3 (Figure 3B, top panel, lanes 4 and 6). The intermediate was also recognized by anti-Myc antibody (Figure 3B, lower panel, lane 5), indicating the existence of the Flag-$Uba5^{C250S}$–Myc-Ufm1 complex. Note that the small-sized intermediate is presumably a complex with an endogenous Ufm1, as mentioned. These results indicate that Uba5 forms an intermediate with Ufm1 and the Gly^{83} residue of Ufm1 is essential for the formation of the intermediate with Uba5 *in vivo*.

We subsequently tested whether Uba5 can activate Ufm1 *in vitro*. The thioester formation assay was performed using recombinant proteins expressed in *Escherichia coli*. Recombinant GST-tagged Uba5 and mature Ufm1

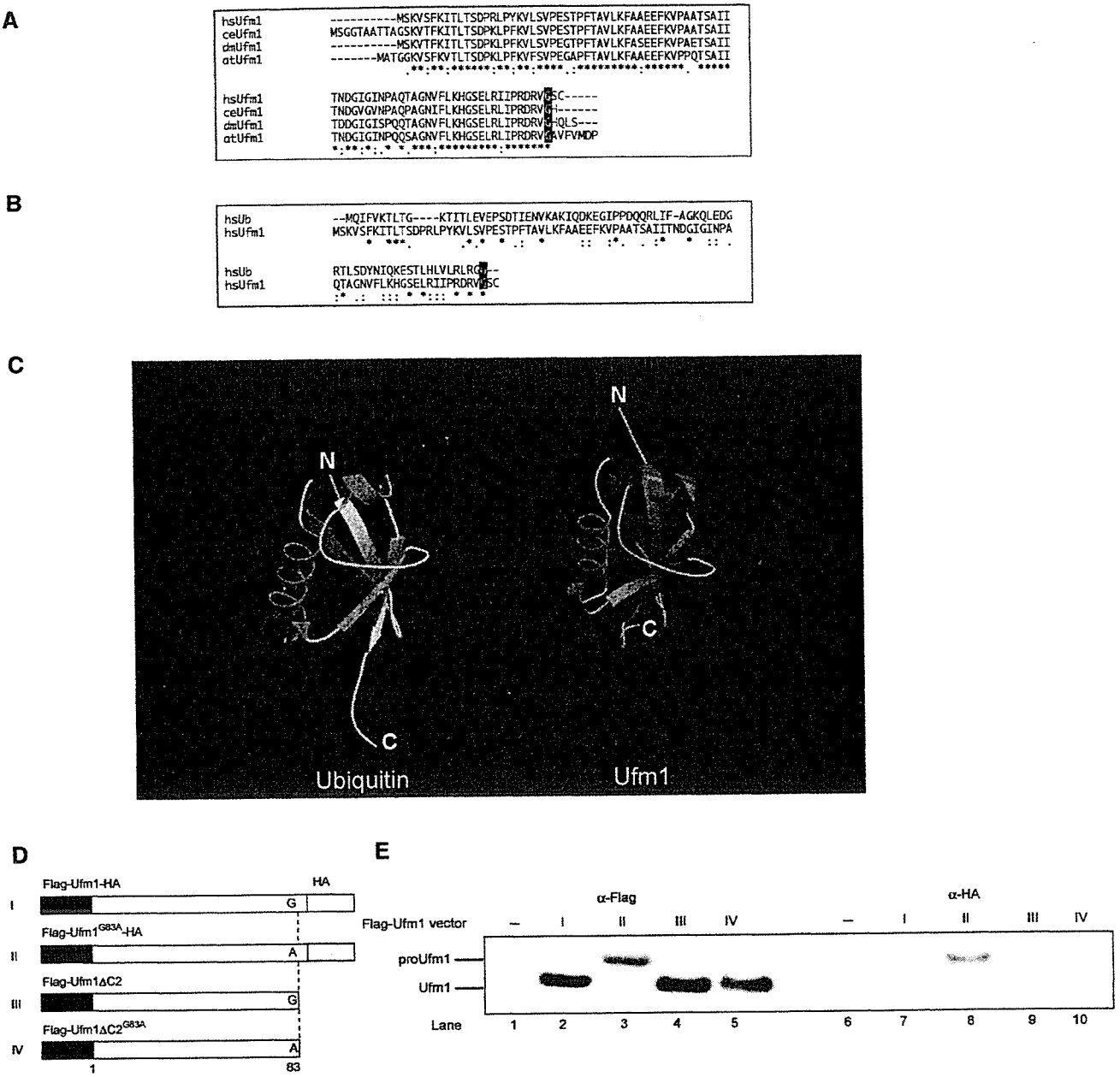

Figure 2 Ufm1, a novel ubiquitin-fold molecule. (**A**) Sequence alignment of hsUfm1 and its homologs. The sequence of hsUfm1 is available from GenBank^{TM} under the accession number BC005193 (dm, a coding region of dmUfm1 was found from *D. melanogaster* genomic sequence; ce, NM_066304; at, NM_106420). The homology analysis was performed as described in Figure 1B. The C-terminal conserved Gly residue is boxed in black. (**B**) Sequence alignment of hsUbiquitin with hsUfm1. The homology analysis was performed as described in Figure 1B. The C-terminal conserved Gly residue is boxed in black. (**C**) Structural ribbon of hsUbiquitin and predicted structural ribbon of hsUfm1. α-Helices and β-strands are shown in green and yellow, respectively. The homology model of hsUfm1 was created from the *C. elegans* Ufm1 structure (Cort *et al*, 2002) by using MOE program (2003.02; Chemical Computing Group Inc., Montreal, Quebec, Canada). (**D**) Schematic representation of mammalian expression plasmids for Ufm1 and the derivative mutants. Flag epitope tags at the N-terminus, HA epitope tags at the C-terminus, and putative cleavage site Gly^{83} residue (vertical dotted lines) are indicated. To construct Ufm1^{G83A}, a single point mutation was introduced into Ufm1, which led to an amino-acid substitution from Gly to Ala at position 83. To construct Ufm1ΔC2, the two C-terminal residues were deleted by PCR. Ufm1ΔC2^{G83A} was also produced by site-directed mutagenesis of Ufm1ΔC2. The ΔC2 mutants were tagged with the Flag epitopes at N-terminus. (**E**) ProUfm1 processing. HEK293 cells were transfected with Flag-Ufm1-HA, Flag-Ufm1^{G83A}-HA, Flag-Ufm1ΔC2, or Flag-Ufm1ΔC2^{G83A}. The cell lysates were subjected to SDS–PAGE and analyzed by immunoblots with anti-Flag and anti-HA antibodies. ProUfm1 and mature Ufm1 are indicated on the left. The numbers at the top from I to IV are similar to those in (D).

(Ufm1ΔC2) with exposed C-terminal Gly^{83} residue were purified, mixed and incubated in the presence of ATP and then subjected to SDS–PAGE at either reducing or nonreducing conditions. GST-Ufm1ΔC3 was used as control. An ~100 kDa band corresponding to the GST-Ufm1ΔC2–GST-Uba5 intermediate complex was clearly observed when the mixture was applied at nonreducing conditions (Figure 3C, lane 3). This intermediate was not observed when ATP or GST-Uba5 was excluded from the mixture (Figure 3C, lanes 1 and 2), or when the mixture was loaded in the presence of

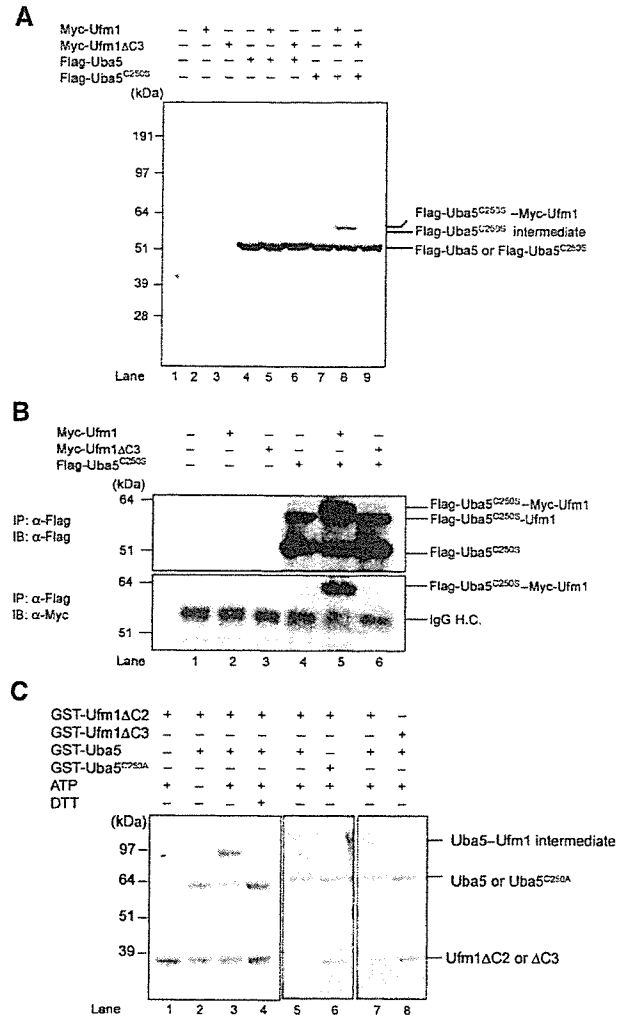

Figure 3 Demonstration that Uba5 is an Ufm1-activating enzyme. (**A**) Immunoblotting analysis. Each Myc-tagged Ufm1 (Myc-Ufm1) and Myc-Ufm1ΔC3 was expressed alone (lanes 2 and 3, respectively), and coexpressed with Flag-Uba5 (lanes 5 and 6, respectively) or Flag-Uba5^{C250S} (lanes 8 and 9, respectively). Each Flag-Uba5 and Flag-Uba5^{C250S} was also expressed alone (lanes 4 and 7, respectively). The cell lysates were subjected to SDS–PAGE and analyzed by immunoblotting with anti-Flag antibody. The bands corresponding to Flag-Uba5, Flag-Uba5^{C250S}, and Flag-Uba5^{C250S} intermediates are indicated on the right. (**B**) Immunoblotting analysis after immunoprecipitation. Each Myc-Ufm1 and Myc-Ufm1ΔC3 was expressed alone (lanes 2 and 3, respectively), and coexpressed with Flag-Uba5^{C250S} (lanes 5 and 6, respectively). Flag-Uba5^{C250S} was also expressed alone (lane 4). The cell lysates were immunoprecipitated with anti-Flag antibody. The resulting immunoprecipitates were subjected to SDS–PAGE and analyzed by immunoblotting with anti-Flag and anti-Myc antibodies. The bands corresponding to Flag-Uba5^{C250S}, Flag-Uba5^{C250S}–endogenous Ufm1, and Flag-Uba5^{C250S}–Myc-Ufm1 intermediates are indicated. (**C**) *In vitro* activating assay of Ufm1 by Uba5. Purified recombinant GST-Ufm1ΔC2 (2 μg) (lanes 1–7) was incubated for 30 min at 25°C with some of the following: 2 μg of purified recombinant GST-Uba5 (lanes 2–5, 7, and 8), GST-Uba5^{C250A} (lane 6), and 5 mM ATP (lanes 1 and 3–8). Lane 8 was conducted similar to lane 7, except that GST-Ufm1ΔC3 was used instead of GST-Ufm1ΔC2. Reactions were then incubated with SDS loading buffer lacking reducing agent (lanes 1–3 and 5–8) or containing 100 mM DTT (lane 4). The presence or absence of various components is indicated above the lanes. The bands corresponding to free GST-Uba5, GST-Uba5^{C250A}, GST-Ufm1ΔC2 (mature Ufm1), GST-Ufm1ΔC3, and GST-Uba5–GST-Ufm1ΔC2 thioester product are indicated on the right.

a reducing agent dithiothreitol (DTT) (Figure 3C, lane 4). Furthermore, GST-tagged Uba5^{C250A} mutant, a presumptive active site Cys mutant, could not form the intermediate even at nonreducing conditions (Figure 3C, lane 6). GST-tagged Ufm1ΔC3 was also incapable of forming the intermediate in this reaction (Figure 3C, lane 8). Taken together, we concluded that Uba5 is an Ufm1-activating enzyme and has the active site in Cys^{250}.

Identification of a novel protein-conjugating enzyme, Ufc1

The LC–MS/MS analysis revealed CGI-126 protein as another Uba5 interacting protein. CGI-126 is a protein of 167-amino-acid residues with a predicted molecular mass of 19.4 kDa. This protein is also conserved in multicellular organisms, like Uba5 and Ufm1 (Figure 4A). The C-terminal half of human CGI-126 has a high identity across species as shown in Figure 4A. CGI-126 has a highly conserved region, for example, residues 113–126, with limited similarity to the region of Ubc's that encodes an active site Cys residue capable of forming a thioester bond (Figure 4A). We assumed that this protein may be an E2-like conjugating enzyme for Ufm1 and thus named it Ufm1-conjugating enzyme 1 (Ufc1). If Ufc1 is an authentic E2 enzyme for Ufm1, it is expected to form an intermediate complex with Ufm1 via a thioester linkage. To test this possibility in the same way as Uba5, we mutated the predicted active site Cys residue within Ufc1 (Figure 4A, Cys^{116}) to Ser. We expressed Flag-Ufc1 or Flag-Ufc1^{C116S} (a presumptive active site Cys at position 116 was replaced by Ser) in combination with Myc-Ufm1 or Myc-Ufm1ΔC3 in HEK293 cells. Flag-Ufc1^{C116S} formed a stable intermediate band when coexpressed with Myc-Ufm1 (Figure 4B, lane 8), but not alone or with Myc-Ufm1ΔC3 (Figure 4B, lanes 7 and 9). To ascertain that this is the Flag-Ufc1^{C116S}–Myc-Ufm1 intermediate, Flag-Ufc1^{C116S} was immunoprecipitated and blotted with anti-Myc antibody (Figure 4C). Indeed, Myc-Ufm1, but not Myc-Ufm1ΔC3, formed a complex with Flag-Ufc1^{C116S} (Figure 4C, lanes 5 and 6, top and bottom panels). Note that Flag-Ufc1^{C116S} intermediate with a faster electrophoretic mobility than the Flag-Ufc1^{C116S}–Myc-Ufm1 complex is presumably the intermediate with the endogenous Ufm1 (Figure 4C, lanes 4–6, upper panel). These results indicate that Ufc1 forms an intermediate with Ufm1 *in vivo*.

To confirm that Ufc1 is indeed an E2-like enzyme that conjugates with Ufm1 *via* a thioester linkage, we conducted an *in vitro* Ufm1 conjugation assay. Recombinant GST-Uba5, GST-Ufc1, and GST-Ufm1ΔC2 were mixed and incubated in the presence of ATP. GST-Ufc1^{C116A} mutant and GST-Ufm1ΔC3 were used as negative controls. Under nonreducing conditions, an ~70 kDa band corresponding to GST-Ufm1ΔC2–GST-Ufc1 intermediate was observed (Figure 4D, lane 4). This product was not formed at reducing conditions, or when any of the components was omitted from the reaction (Figure 4D, lanes 1–3 and 5). GST-tagged Ufc1^{C116A} mutant could not form the intermediate, suggesting that Cys116 is indeed the active site (Figure 4D, lane 7). GST-Ufm1ΔC3 was again unable to form the intermediate complex in this reaction (Figure 4D, lane 9). Taken together, we concluded that Ufc1 functions as an Ufm1-conjugating enzyme and has the active site in Cys^{116}.

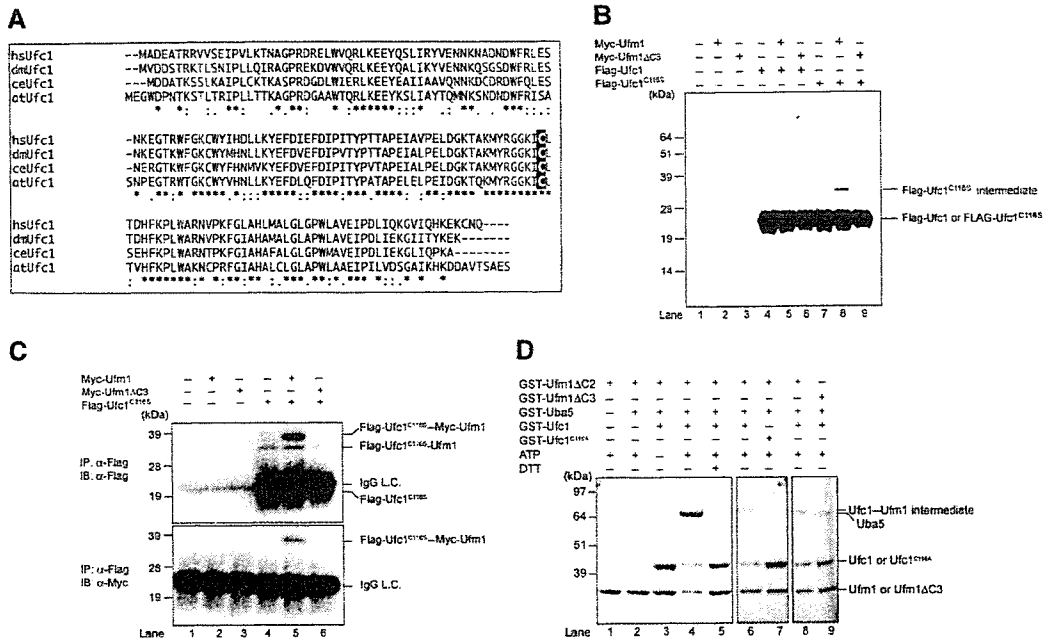

Figure 4 Ufc1, a novel E2-like enzyme. (**A**) Sequence alignment of hsUfc1 and its homologs. The sequence of Ufc1 is available from GenBank™ under the accession number BC005187 (dm, NM_137230; ce, NM_066654; at, BT001180). The homology analysis was performed as described in Figure 1B. The putative active site Cys residue is boxed in black. (**B**) Immunoblotting analysis. Each Myc-tagged Ufm1 (Myc-Ufm1) and Myc-Ufm1ΔC3 was expressed alone (lanes 2 and 3, respectively), and coexpressed with Flag-Ufc1 (lanes 5 and 6, respectively) or Flag-Ufc1^{C116S} (lanes 8 and 9, respectively). Each Flag-Ufc1 and Flag-Ufc1^{C116S} was also expressed alone (lanes 4 and 7, respectively). The cell lysates were subjected to SDS–PAGE and analyzed by immunoblotting with anti-Flag antibody. The bands corresponding to Flag-Ufc1, Flag-Ufc1^{C116S}, and Flag-Ufc1^{C116S} intermediates are indicated on the right. (**C**) Immunoblotting analysis after immunoprecipitation. Each Myc-Ufm1 and Myc-Ufm1ΔC3 was expressed alone (lanes 2 and 3, respectively), and coexpressed with Flag-Ufc1^{C116S} (lanes 5 and 6, respectively). Flag-Ufc1^{C116S} was also expressed alone (lane 4). The cell lysates were immunoprecipitated with anti-Flag antibody. The resulting immunoprecipitates were subjected to SDS–PAGE and analyzed by immunoblots with anti-Flag and anti-Myc antibodies. The bands corresponding to Flag-Ufc1^{C116S}, Flag-Ufc1^{C116S}–endogenous Ufm1, and Flag-Ufc1^{C116S}–Myc-Ufm1 intermediates are indicated. (**D**) *In vitro* thioester bond formation assay of Ufm1 by Ufc1. Purified recombinant GST-Ufm1ΔC2 (2 μg) (lanes 1–8) was incubated for 30 min at 25°C with the following: purified recombinant GST-Uba5 (0.2 μg) (lanes 2–9), GST-Ufc1 (2 μg) (lanes 3–6, 8, and 9), GST-Ufc1^{C116S} (2 μg) (lane 7), and 5 mM ATP (lanes 1, 2, and 4–9). Lane 9 was conducted similar to lane 8, except that GST-Ufm1ΔC3 was used instead of GST-Ufm1ΔC2. Reactions were then incubated with SDS loading buffer lacking reducing agent (lanes 1–4 and 6–9) or containing 100 mM DTT (lane 5). The presence or absence of various components is indicated above the lanes. The bands corresponding to free GST-Ufm1ΔC2 (mature Ufm1), GST-Ufm1ΔC3, GST-Uba5, GST-Ufc1, GST-Ufc1^{C116S}, and GST-Ufc1–GST-Ufm1ΔC2 thioester product are indicated on the right.

Conjugation of Ufm1 to cellular protein(s)

We next examined whether Ufm1 conjugates to the target protein(s) in cells. To this end, we expressed Flag- and 6xHis-tagged Ufm1 constructs in HEK293 cells, and purified them under denaturing conditions by Ni^{2+} beads. The resulting precipitates were then analyzed by immunoblotting with anti-Flag antibody. When FlagHis-Ufm1-HA (proUfm1) or FlagHis-Ufm1ΔC2 (mature form) was expressed, several proteins with sizes of about 28, 38, and 47 kDa were detected, in addition to the 10 kDa corresponding to free FlagHis-Ufm1ΔC2 (Figure 5A, lanes 2 and 4). These bands were not detected by FlagHis-Ufm1^{G83A}-HA and FlagHis-Ufm1ΔC3, suggesting that both C-terminal cleavage and C-terminal Gly residue are required for the conjugation reaction (Figure 5A, lanes 3 and 6). Moreover, these protein bands were resistant to reducing agents, such as DTT and β-mercaptoethanol. These results indicate that Ufm1 is covalently attached to some target proteins, probably through an isopeptide bond between the C-terminal Gly^{83} of Ufm1 and a Lys residue in the cellular proteins. It is of note that FlagHis-Ufm1^{G83A} mutant with exposed C-terminal Ala instead of Gly can conjugate to target proteins (Figure 5A, lane 5), consistent with the previous report on ubiquitin and SUMO (Hodgins *et al*, 1992; Kamitani *et al*, 1997). Since C-terminal Gly to Ala mutation confers resistance to the Ufm1 processing, the conjugates with FlagHis-Ufm1^{G83A} mutant may be more stable than those with FlagHis-Ufm1ΔC2 (Figure 5A, compare lanes 4 and 5). These results suggest that the Ufm1 conjugation is also a reversible reaction.

We further investigated the expression of Ufm1 and its conjugated proteins in mouse tissues using anti-Ufm1 serum. Ufm1 was widely expressed in all tissues examined, such as brain, heart, lung, liver, and kidney (Figure 5B, left panel). In addition, several bands with striking similarity to proteins detected in HEK293 cells were observed. These bands were not detected by preimmune or preabsorbed antisera (Figure 5B, right panel), suggesting that they are likely the Ufm1 conjugates. Although the intensity of each band varied among tissues and HEK293 cells, 28 and 38 kDa proteins were commonly detected. The 70-kDa band observed in all tissues was also detected faintly in HEK293 cells (Figure 5A, lane 5). The 47-kDa band observed in HEK293 cells was not clear. These protein bands were resistant to reducing agents, such as DTT and β-mercaptoethanol, indicating that Ufm1 covalently attaches to cellular proteins like other Ubl proteins. The targets of Ufm1 appeared to be common in a variety

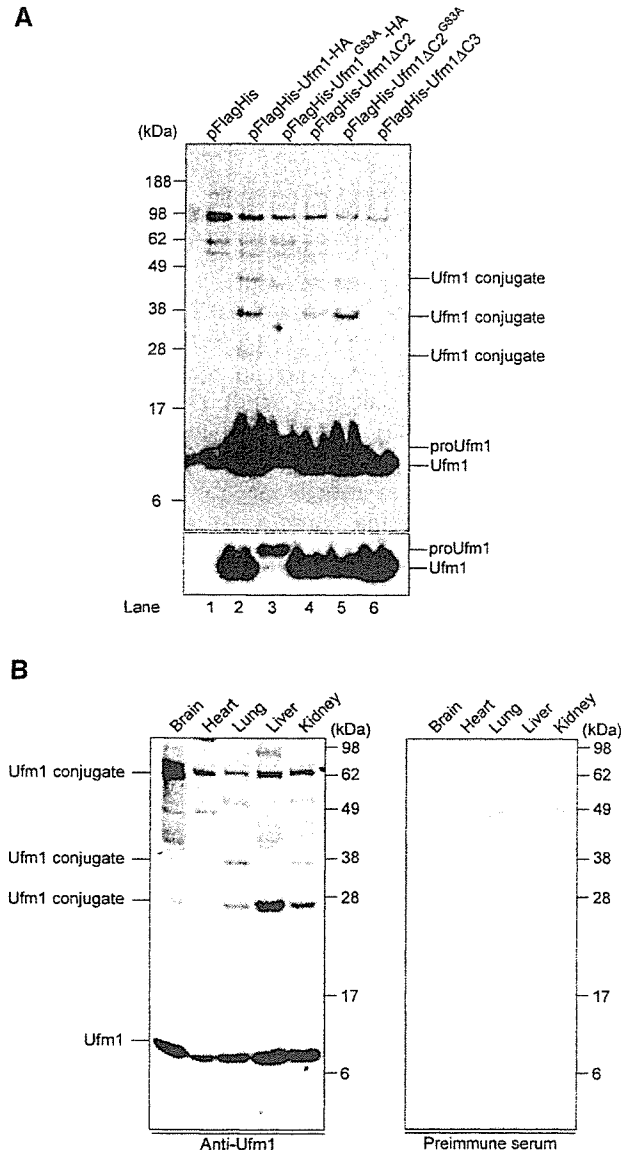

Figure 5 Formation of a covalent protein conjugate(s) with Ufm1 in HEK293 cells and mouse tissues. (**A**) Ufm1 conjugates in human HEK293 cells. HEK293 cells were transfected with FlagHis-Ufm1-HA, FlagHis-Ufm1^{G83A}-HA, FlagHis-Ufm1ΔC2, FlagHis-Ufm1ΔC2^{G83A}, or FlagHis-Ufm1ΔC3 expression plasmids. These cells were lysed under denaturing conditions, and the lysates were precipitated with Ni^{2+} beads. The precipitates were subjected to SDS–PAGE and analyzed by immunoblotting with anti-Flag antibody. The bottom panel shows the short exposure of the upper panel. The bands corresponding to mature Ufm1, proUfm, and Ufm1 conjugates are indicated on the right. (**B**) Ufm1 conjugates in various mouse tissues. Homogenates from mouse tissues as indicated were prepared and subjected to SDS–PAGE and analyzed by immunoblotting with anti-Ufm1 serum (left panel) or preimmune serum (right panel). The bands corresponding to Ufm1 and conjugates between Ufm1 and target proteins are indicated on the left.

of tissues. These results suggest the universal roles of Ufm1 in the regulation of cellular function in multicellular organisms.

Subcellular localization of Ufm1 in HeLa cells

We finally examined the subcellular distribution of Ufm1 in HeLa cells. Immunocytochemical analysis using anti-Ufm1

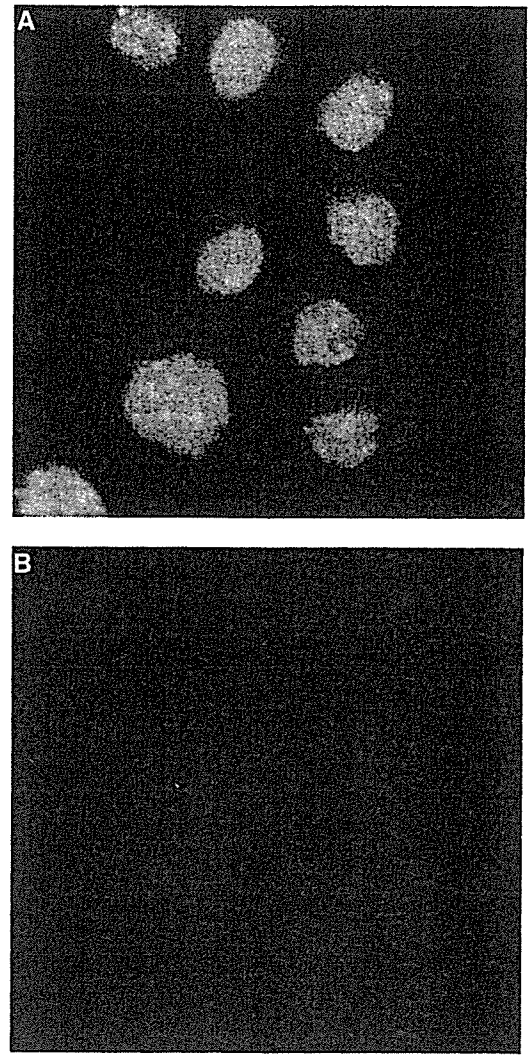

Figure 6 Intracellular distribution of Ufm1 in HeLa cells. (**A**) HeLa cells were seeded on coverslips 24 h before fixation for immunostaining. Ufm1 was detected with anti-Ufm1 serum and visualized with Alexa 488 nm anti-rabbit antibody. (**B**) Immunocytochemical analysis was conducted as for (A), except that preimmune serum was used. Cells were observed using a fluorescence microscope. Magnification, × 400.

serum revealed that Ufm1 was predominantly localized in the nucleus and diffusely in the cytoplasm (Figure 6A). These staining patterns were not observed when anti-Ufm1 serum had been preadsorbed with excess amounts of recombinant Ufm1 protein or preimmune serum was used instead of anti-Ufm1 serum (Figure 6B). Moreover, Ufm1 localization in the cytoplasm and nucleus was similar to the localization of exogenously expressed GFP-tagged Ufm1 in HeLa cells (data not shown). In the nucleus, strong immunoreactivity to anti-Ufm1 serum was observed as a dot-like structure. Although such dots-like structures were detected by preimmune serum, those intensities were weak. Thus, some of these dot-like structures may represent conjugates of Ufm1.

Discussion

In the present study, we reported that Ufm1 acts as a new post-translational UBL modifier, based on the following

criteria: (1) It is a small protein of 9.1 kDa with a ubiquitin-fold structure. (2) Ufm1 is synthesized in a precursor form, and the extra amino-acid residues at the C-terminal side need to be processed to expose the Gly residue. (3) The C-terminal processing and exposure of glycine residue are essential to the formation of Ufm conjugates in the cells. (4) Ufm1 has specific E1-like (Uba5) and E2-like (Ufc1) enzymes for activation and conjugation, respectively. Intriguingly, many UBL modifiers are evolutionarily conserved from yeast to human, except interferon-inducible UBL modifiers, such as UCRP/ISG15, Fat10, and Fau1/MNSFβ (Nakamura *et al*, 1995; D'Cunha *et al*, 1996; Liu *et al*, 1999). Ufm1, Uba5, and Ufc1 found in the present study are conserved in various multicellular organisms (Figures 1B, 2A, and 4A), but not in both budding and fission yeasts, suggesting that they all have been generated by coevolution.

We identified Uba5 as an E1 enzyme for Ufm1. This enzyme is relatively small compared to Uba1, that is, an E1 for ubiquitin (Figure 1A). In the *in vitro* assay, the recombinant Uba5 protein formed a thioester linkage with recombinant Ufm1 (Figure 3C) and transferred the activated Ufm1 to recombinant Ufc1 (an E2 enzyme) (Figure 4D), indicating that Uba5 can activate Ufm1 as a single molecule. This is in marked contrast to other E1s such as Uba2 and Uba3, which retain obvious similarities to the C-terminal half of Uba1 but require the formation of heterodimer complexes with respective partner molecules, AOS1 and APP-BP1, respectively, with similarities to the N-terminal half of Uba1 (Johnson *et al*, 1997; Liakopoulos *et al*, 1998; Osaka *et al*, 1998). Another E1-like enzyme, Uba4 that activates Urm1, is of similar size to Uba5 (Furukawa *et al*, 2000), but it remains unknown whether Uba4 acts as a single molecule or needs a partner subunit. The homology of Uba5 to Uba1 is less than those of Uba2 and Uba3, except their ThiF domain conserved in E1s, and thus it is likely that Uba5 may uniquely activate Ufm1, differing from other E1s such as Uba1, Uba2/AOS1, and Uba3/APP-BP1. Thus, although the structure of APP-BP1/Uba3 heterodimer is determined and the mechanism by which E1s activate their cognate UBLs was proposed (Walden *et al*, 2003a, b), the weak homology of Uba5 with other E1s hampered the computer-assisted structural analysis. To clarify this issue, structural analysis of Uba5 is required. This issue is currently under investigation in our laboratories. So far, most E1-like enzymes activate single species of UBL protein, although Atg7 is exception, which can activate both Atg8 and Atg12 (Mizushima *et al*, 1998; Tanida *et al*, 1999; Ichimura *et al*, 2000). A total of 10 E1-like enzymes can be identified in the human genome by computer analysis. Considering the limited number of E1-like proteins, it is possible that some E1-like proteins can activate a distinct set of UBL proteins. Whether or not Uba5 is capable of activating proteins other than Ufm1 remains to be clarified.

There are more than a dozen of E2 family genes in human genomes. In the budding yeast, 13 different E2s, namely Ubc1–Ubc13, have been documented and functionally characterized. Functionally, most of them catalyze the conjugation of ubiquitin, except that Ubc9 and Ubc12 are for SUMO and NEDD8/Rub1, respectively (Johnson and Blobel, 1997; Lammer *et al*, 1998; Osaka *et al*, 1998). In addition, in the autophagic pathway, Atg3 and Atg10 are both E2 enzymes for Atg8 and Atg12, respectively, but they do not have obvious sequence similarities to known Ubc's, except for a short region encompassing an active Cys residue (Shintani *et al*, 1999; Ichimura *et al*, 2000). Similarly, Ufc1 is a unique E2-like enzyme with no obvious sequence homology with other E2s, except approximately 10 amino-acid residues encompassing the active site Cys residue.

In assessing the biological roles of the Ufm1-modifying system, characterization of the target molecule(s) is of particular importance. Regarding this issue, we identified several putative proteins that are conjugated with Ufm1 in human HEK293 cells and various mouse tissues. It is noteworthy that the sizes of these bands (28, 38, 47 kDa) increase by 10 kDa, which is consistent with the size of Ufm1. Considering that several Ubl modifiers can attach to target proteins as a polymer, it is possible that these bands correspond to multi- or poly-Ufm1 conjugates. In fact, Ufm1 has six Lys residues. Whether Ufm1 is conjugated to several distinct proteins or multiple Lys residues in a single target or polymerized in a single Lys residue awaits future study. Unfortunately, we could not identify the protein, and detailed analysis of the cellular function of Ufm1 conjugation awaits future study. It was recently reported that Uba5 is induced by certain reagents that induce stress in the endoplasmic reticulum (ER), a so-called 'unfolded protein response' (Harding *et al*, 2003). However, we could not observe the induction of Uba5, Ufc1, and Ufm1 by treatment with various compounds known to induce ER stress in mammalian cells (data not shown). In addition, exposure to other stresses including high temperature or heavy metals also did not induce the appearance of obvious new conjugation band(s) of Ufm1, by immunoblot analysis. Further studies on the biological roles of the Ufm1 conjugation pathway are under investigation in our laboratories.

Materials and methods

DNA construction

The cDNA encoding human Uba5 was obtained by PCR from human liver cDNA with the Uba5-s5′ primer (5′-CGGAGGGATCCC CATGGCGGAGTCTGTGGAG-3′) and the Uba5-r3′ primer (5′-CAGTCCTCGAGCTACATATTCTTCATTTT-3′). It was then subcloned into pcDNA3 vector (Invitrogen, San Diego, CA). A point mutation for Cys at position 250 to Ser or Ala was generated by PCR-based site-directed mutagenesis. The Flag tag was introduced at the N-terminus of Uba5 or Uba5^{C250S}. Similarly, cDNA encoding human Ufm1 was amplified by PCR from human liver cDNA with the Ufm1-s5′ primer (5′-TTCCGGGATCCCCATGTCGAAGGTTTCCTTT-3′) and the Ufm1-r3′ primer (5′-AGTAGCTCGAGTTAACAACTTCCAA CACGAT-3′), and subcloned into pcDNA3 vector. The Flag, FlagHis, or Myc tags were introduced at the N-terminus of Ufm1. The HA tag was introduced at the C-terminus of Ufm1. The C-terminal deletion mutants of Ufm1 named Ufm1ΔC2 and Ufm1ΔC3, encoding amino acids 1–83 and 1–82, respectively, were generated by PCR. A point mutation for Gly at position 83 to Ala of Ufm1 and Ufm1ΔC2 (Ufm1^{G83A} and Ufm1ΔC2^{G83A}, respectively) was generated by PCR-based site-directed mutagenesis. The cDNA encoding human Ufc1 was obtained by PCR from human liver cDNA with the Ufc1-s5′ primer (5′-GCCCTGGATCCAGATGGCGGATGAAGCCACG-3′) and the Ufc1-r3′ primer (5′-TTCTCGAGTCATTGGTTGCATTTCTCTT-3′). It was then subcloned into pcDNA3 vector. A point mutation for Cys at position 116 to Ser or Ala was generated by PCR-based site-directed mutagenesis. The Flag tag was introduced at the N-terminus of Ufc1 and Ufc1^{C116S}. To express GST-fused Ufm1ΔC2, Ufm1ΔC3, Uba5, Uba5^{C250A}, Ufc1, and Ufc1^{C116A} in *E. coli*, these cDNAs were subcloned into pGEX-6p vector (Amersham Biosciences). All mutations mentioned above were confirmed by DNA sequencing.

Cell culture and transfection

Media and reagents for cell culture were purchased from Life Technologies (Grand Island, NY). HEK293 cells were grown in Dulbecco's modified Eagle's medium (DMEM) containing 10% fetal calf serum (FCS), 5 U/ml penicillin, and 50 μg/ml streptomycin. HEK293 cells at subconfluence were transfected with the indicated plasmids using Fugene 6 reagent (Roche Molecular Biochemicals, Mannheim, Germany). Cells were analyzed at 20–24 h after transfection.

Immunological analysis

For immunoblot analysis, cells were lysed with ice-cold TNE buffer (10 mM Tris–HCl, pH 7.5, 1% Nonidet P-40, 150 mM NaCl, 1 mM ethylenediaminetetraacetic acid (EDTA), and protease inhibitors) and the lysates were separated by SDS–PAGE (12% gel or 4–12% gradient gel) and transferred to a polyvinylidene difluoride (PVDF) membrane. Mouse monoclonal anti-Flag antibody (M2; Sigma Chemical Co., St Louis, MO), anti-HA antibody (F7; Santa Cruz Biotechnology, Santa Cruz, CA), and rabbit polyclonal anti-Myc antibody (N14; Santa Cruz) were used for immunodetection. Development was performed by the Western lighting detection methods.

For immunoprecipitation analysis, cells were lysed by 200 μl of TNE, and the lysate was then centrifuged at 10 000 *g* for 10 min at 4°C to remove debris. In the next step, 800 μl of TNE and 30 μl of M2-agarose (Sigma) were added to the lysate, and the mixture was mixed under constant rotation for 12 h at 4°C. The immunoprecipitates were washed five times with ice-cold TNE. The complex was boiled for 10 min in SDS sample buffer in the presence of β-mercaptoethanol to elute proteins and centrifuged at 10 000 *g* for 10 min at 4°C. The supernatant was subjected to SDS–PAGE, transferred to PVDF membrane, and analyzed by immunoblots with anti-Flag (M2) or anti-Myc (N14) antibody.

For purification of 6xHis-tagged proteins under denaturing conditions, cells were lysed by 1 ml of denaturing lysis buffer (8 M urea, 0.1 M NaH_2PO_4, and 0.01 M Tris–HCl, pH 8.0) in the presence of 20 mM *N*-ethylmaleimide as an inhibitor of isopeptidases, and the lysate was sonicated briefly and then centrifuged at 10 000 *g* for 10 min at room temperature to remove debris. Then, 30 μl of Ni-NTA Superflow (QIAGEN) was added to the lysate, and the mixture was shaken under constant rotation for 30 min at room temperature. The precipitates were washed five times with denaturing wash buffer (8 M urea, 0.1 M NaH_2PO_4, and 0.01 M Tris–HCl, pH 5.9). To elute proteins, elution buffer (8 M urea, 0.1 M NaH_2PO_4, and 0.01 M Tris–HCl, pH 4.5) was added to the complex, and the mixture was centrifuged at 10 000 *g* for 10 min at room temperature. The resulting supernatant was subjected to SDS–PAGE, transferred to PVDF membrane, and analyzed by immunoblots with anti-Flag (M2).

Freshly isolated tissues from mice were homogenized in lysis buffer (50 mM Tris–HCl, pH 7.5, 1% SDS, 5 mM EDTA, and 10 mM β-mercaptoethanol) using potter-Elvehjem homogenizer. The homogenate was centrifuged at 10 000 *g* for 10 min to remove debris. The resulting supernatant was subjected to SDS–PAGE, transferred to PVDF membrane, and analyzed by immunoblotting with anti-Ufm1 or preimmune serum. The anti-Ufm1 polyclonal antibody was raised in rabbits using the recombinant protein produced in *E. coli* as an antigen.

In vitro thioester formation assay

Recombinant GST-Ufm1ΔC2, GST-Ufm1ΔC3, GST-Uba5, GST-Uba5^{C250A}, GST-Ufc1, and GST-Ufc1^{C116A} (tagged N-terminally with GST) were produced in *E. coli* and recombinant proteins were purified by chromatography on glutathione sepharose 4B (Amersham Biosciences). After elution of proteins from the beads, the preparations were dialyzed against 50 mM BisTris (pH 6.5), 100 mM NaCl, 10 mM $MgCl_2$, and 0.1 mM DTT (reaction buffer). Most thioester formation reactions contained reaction buffer with 4 μg GST-Ufm1ΔC2 or GST-Ufm1ΔC3 and some of the following: 5 mM ATP, 2 or 0.2 μg GST-Uba5 or GST-Uba5^{C250A}, and 4 μg GST-Ufc1 or GST-Ufc1^{C116A}. Reactions were incubated for 30 min at 25°C and stopped by the addition of SDS-containing loading buffer either lacking reducing agent or containing 100 mM DTT, followed by a 10 min incubation at 37°C, SDS–PAGE (4–12% acrylamide gradient) and Coomassie brilliant blue staining.

Protein identification by LC–MS/MS analysis

The Uba5-associated complexes were digested with *Achromobacter* protease I and the resulting peptides were analyzed using a nanoscale LC–MS/MS system as described previously (Natsume *et al*, 2002). The peptide mixture was applied to a Mightysil-PR-18 (1 μm particle, Kanto Chemical) frit-less column (45 mm × 0.150 mm ID) and separated using a 0–40% gradient of acetonitrile containing 0.1% formic acid over 30 min at a flow rate of 50 nl/min. Eluted peptides were sprayed directly into a quadropole time-of-flight hybrid mass spectrometer (Q-Tof *Ultima*, Micromass, Manchester, UK). MS and MS/MS spectra were obtained in a data-dependent mode. Up to four precursor ions above an intensity threshold of 10 counts/s were selected for MS/MS analyses from each survey scan. All MS/MS spectra were searched against protein sequences of Swiss Prot and RefSeq (NCBI) using batch processes of Mascot software package (Matrix Science, London, UK). The criteria for match acceptance were the following: (1) When the match score was 10 over each threshold, identification was accepted without further consideration. (2) When the difference of score and threshold was lower than 10, or when proteins were identified based on a single matched MS/MS spectrum, we manually confirmed the raw data prior to acceptance. (3) Peptides assigned by less than three y series ions and peptides with +4 charge state were all eliminated regardless of their scores.

Immunofluorescence

HeLa cells grown on glass coverslips were fixed in 4% paraformaldehyde (PFA) in PBS for 15 min, and permeabilized with 0.2% (vol/vol) Triton X-100 in PBS for 30 min. After permeabilization, the cells were blocked for 30 min with 5% (vol/vol) normal goat serum in PBS, incubated for 1 h at 37°C with anti-Ufm1 serum or preimmune serum, washed with PBS, and incubated for 30 min with Alexa 488 nm anti-rabbit antibodies (Molecular Probes). The coverslips were washed and mounted on slides. Fluorescence images were obtained using a fluorescence microscope (DMIRE2; Leica) equipped with a cooled charge-coupled device camera (CTR MIC; Leica). Pictures were taken using Leica Qfluoro software (Leica).

Acknowledgements

We thank T Mizushima (Nagoya University) for the computer-assisted structural modeling of human Ufm1. This work was supported in part by Grants-in-Aid from the Ministry of Education, Culture, Sports, Science and Technology of Japan.

References

Bonifacino JS, Weissman AM (1998) Ubiquitin and the control of protein fate in the secretory and endocytic pathways. *Annu Rev Cell Dev Biol* **14:** 19–57

Cort JR, Chiang Y, Zheng D, Montelione GT, Kennedy MA (2002) NMR structure of conserved eukaryotic protein ZK652.3 from *C. elegans*: a ubiquitin-like fold. *Proteins* **48:** 733–736

D'Cunha J, Knight Jr E, Haas AL, Truitt RL, Borden EC (1996) Immunoregulatory properties of ISG15, an interferon-induced cytokine. *Proc Natl Acad Sci USA* **93:** 211–215

Furukawa K, Mizushima N, Noda T, Ohsumi Y (2000) A protein conjugation system in yeast with homology to biosynthetic enzyme reaction of prokaryotes. *J Biol Chem* **275:** 7462–7465

Glickman MH, Ciechanover A (2002) The ubiquitin–proteasome proteolytic pathway: destruction for the sake of construction. *Physiol Rev* **82:** 373–428

Harding HP, Zhang Y, Zeng H, Novoa I, Lu PD, Calfon M, Sadri N, Yun C, Popko B, Paules R, Stojdl DF, Bell JC, Hettmann T, Leiden JM, Ron D (2003) An integrated stress response regulates amino

acid metabolism and resistance to oxidative stress. *Mol Cell* **11:** 619–633

Hershko A, Ciechanover A (1998) The ubiquitin system. *Annu Rev Biochem* **67:** 425–479

Hodgins RR, Ellison KS, Ellison MJ (1992) Expression of a ubiquitin derivative that conjugates to protein irreversibly produces phenotypes consistent with a ubiquitin deficiency. *J Biol Chem* **267:** 8807–8812

Ichimura Y, Kirisako T, Takao T, Satomi Y, Shimonishi Y, Ishihara N, Mizushima N, Tanida I, Kominami E, Ohsumi M, Noda T, Ohsumi Y (2000) A ubiquitin-like system mediates protein lipidation. *Nature* **408:** 488–492

Jentsch S, Pyrowolakis G (2000) Ubiquitin and its kin: how close are the family ties? *Trends Cell Biol* **10:** 335–342

Johnson ES, Blobel G (1997) Ubc9p is the conjugating enzyme for the ubiquitin-like protein Smt3p. *J Biol Chem* **272:** 26799–26802

Johnson ES, Schwienhorst I, Dohmen RJ, Blobel G (1997) The ubiquitin-like protein Smt3p is activated for conjugation to other proteins by an Aos1p/Uba2p heterodimer. *EMBO J* **16:** 5509–5519

Kabeya Y, Mizushima N, Ueno T, Yamamoto A, Kirisako T, Noda T, Kominami E, Ohsumi Y, Yoshimori T (2000) LC3, a mammalian homologue of yeast Apg8p, is localized in autophagosome membranes after processing. *EMBO J* **19:** 5720–5728

Kamitani T, Nguyen HP, Yeh ET (1997) Preferential modification of nuclear proteins by a novel ubiquitin-like molecule. *J Biol Chem* **272:** 14001–14004

Klionsky DJ, Cregg JM, Dunn Jr WA, Emr SD, Sakai Y, Sandoval IV, Sibirny A, Subramani S, Thumm M, Veenhuis M, Ohsumi Y (2003) A unified nomenclature for yeast autophagy-related genes. *Dev Cell* **5:** 539–545

Klionsky DJ, Emr SD (2000) Autophagy as a regulated pathway of cellular degradation. *Science* **290:** 1717–1721

Komatsu M, Tanida I, Ueno T, Ohsumi M, Ohsumi Y, Kominami E (2001) The C-terminal region of an Apg7p/Cvt2p is required for homodimerization and is essential for its E1 activity and E1–E2 complex formation. *J Biol Chem* **276:** 9846–9854

Lammer D, Mathias N, Laplaza JM, Jiang W, Liu Y, Callis J, Goebl M, Estelle M (1998) Modification of yeast Cdc53p by the ubiquitin-related protein rub1p affects function of the SCFCdc4 complex. *Genes Dev* **12:** 914–926

Liakopoulos D, Doenges G, Matuschewski K, Jentsch S (1998) A novel protein modification pathway related to the ubiquitin system. *EMBO J* **17:** 2208–2214

Liu YC, Pan J, Zhang C, Fan W, Collinge M, Bender JR, Weissman SM (1999) A MHC-encoded ubiquitin-like protein (FAT10) binds noncovalently to the spindle assembly checkpoint protein MAD2. *Proc Natl Acad Sci USA* **96:** 4313–4318

Mizushima N, Noda T, Yoshimori T, Tanaka Y, Ishii T, George MD, Klionsky DJ, Ohsumi M, Ohsumi Y (1998) A protein conjugation system essential for autophagy. *Nature* **395:** 395–398

Nakamura M, Xavier RM, Tsunematsu T, Tanigawa Y (1995) Molecular cloning and characterization of a cDNA encoding monoclonal nonspecific suppressor factor. *Proc Natl Acad Sci USA* **92:** 3463–3467

Natsume T, Yamauchi Y, Nakayama H, Shinkawa T, Yanagida M, Takahashi N, Isobe T (2002) A direct nanoflow liquid chromatography–tandem mass spectrometry system for interaction proteomics. *Anal Chem* **74:** 4725–4733

Ohsumi Y (2001) Molecular dissection of autophagy: two ubiquitin-like systems. *Nat Rev Mol Cell Biol* **2:** 211–216

Osaka F, Kawasaki H, Aida N, Saeki M, Chiba T, Kawashima S, Tanaka K, Kato S (1998) A new NEDD8-ligating system for cullin-4A. *Genes Dev* **12:** 2263–2268

Pickart CM (2001) Mechanisms underlying ubiquitination. *Annu Rev Biochem* **70:** 503–533

Schwartz DC, Hochstrasser M (2003) A superfamily of protein tags: ubiquitin, SUMO and related modifiers. *Trends Biochem Sci* **28:** 321–328

Shintani T, Mizushima N, Ogawa Y, Matsuura A, Noda T, Ohsumi Y (1999) Apg10p, a novel protein-conjugating enzyme essential for autophagy in yeast. *EMBO J* **18:** 5234–5241

Tanaka K, Suzuki T, Chiba T (1998) The ligation systems for ubiquitin and ubiquitin-like proteins. *Mol Cells* **8:** 503–512

Tanida I, Komatsu M, Ueno T, Kominami E (2003) GATE-16 and GABARAP are authentic modifiers mediated by Apg7 and Apg3. *Biochem Biophys Res Commun* **300:** 637–644

Tanida I, Mizushima N, Kiyooka M, Ohsumi M, Ueno T, Ohsumi Y, Kominami E (1999) Apg7p/Cvt2p: a novel protein-activating enzyme essential for autophagy. *Mol Biol Cell* **10:** 1367–1379

Varshavsky A (1997) The ubiquitin system. *Trends Biochem Sci* **22:** 383–387

Walden H, Podgorski MS, Huang DT, Miller DW, Howard RJ, Minor Jr DL, Holton JM, Schulman BA (2003a) The structure of the APPBP1–UBA3–NEDD8–ATP complex reveals the basis for selective ubiquitin-like protein activation by an E1. *Mol Cell* **12:** 1427–1437

Walden H, Podgorski MS, Schulman BA (2003b) Insights into the ubiquitin transfer cascade from the structure of the activating enzyme for NEDD8. *Nature* **422:** 330–334

Yeh ET, Gong L, Kamitani T (2000) Ubiquitin-like proteins: new wines in new bottles. *Gene* **248:** 1–14

Developmental Cell, Vol. 6, 661–672, May, 2004, Copyright ©2004 by Cell Press

Skp2-Mediated Degradation of p27 Regulates Progression into Mitosis

Keiko Nakayama,[1,2,5] Hiroyasu Nagahama,[2,3,5] Yohji A. Minamishima,[2,3] Satoshi Miyake,[1,2] Noriko Ishida,[1,2,3] Shigetsugu Hatakeyama,[2,3] Masatoshi Kitagawa,[2,3] Shun-ichiro Iemura,[4] Tohru Natsume,[4] and Keiichi I. Nakayama[2,3,*]
[1]Division of Developmental Genetics
Center for Translational and Advanced Animal Research on Human Diseases
Tohoku University School of Medicine
Sendai, Miyagi 980-8575
Japan
[2]CREST
Japan Science and Technology Corporation (JST)
Kawaguchi, Saitama 332-0012
Japan
[3]Department of Molecular and Cellular Biology
Medical Institute of Bioregulation
Kyushu University
Fukuoka, Fukuoka 812-8582
Japan
[4]National Institute of Advanced Industrial Science and Technology (AIST)
Biological Information Research Center
Tokyo 135-0064
Japan

Summary

Although Skp2 has been thought to mediate the degradation of p27 at the G_1-S transition, *Skp2*$^{-/-}$ cells exhibit accumulation of p27 in S-G_2 phase with overreplication. We demonstrate that *Skp2*$^{-/-}$*p27*$^{-/-}$ mice do not exhibit the overreplication phenotype, suggesting that p27 accumulation is required for its development. Hepatocytes of *Skp2*$^{-/-}$ mice entered the endoduplication cycle after mitogenic stimulation, whereas this phenotype was not apparent in *Skp2*$^{-/-}$*p27*$^{-/-}$ mice. Cdc2-associated kinase activity was lower in *Skp2*$^{-/-}$ cells than in wild-type cells, and a reduction in Cdc2 activity was sufficient to induce overreplication. The lack of p27 degradation in G_2 phase in *Skp2*$^{-/-}$ cells may thus result in suppression of Cdc2 activity and consequent inhibition of entry into M phase. These data suggest that p27 proteolysis is necessary for the activation of not only Cdk2 but also Cdc2, and that Skp2 contributes to regulation of G_2-M progression by mediating the degradation of p27.

Introduction

The highly ordered progression of the cell cycle is achieved by a series of elaborate mechanisms that control the periodic expression of many regulatory proteins. One such regulatory protein is the Cdk inhibitor (CKI) p27. In normal cells, the amount of p27 is high during G_0 phase but rapidly decreases on the reentry of cells into G_1-S. Moreover, we and others have demonstrated that *p27*$^{-/-}$ mice are larger than normal mice and exhibit both multiple organ hyperplasia and a predisposition to the development of tumors (Fero et al., 1996; Kiyokawa et al., 1996; Nakayama et al., 1996).

The intracellular concentration of p27 is thought to be regulated predominantly by the ubiquitin-mediated proteolytic pathway (Pagano et al., 1995; Shirane et al., 1999). Degradation of p27 is promoted by its phosphorylation on Thr^{187} by the cyclin E-Cdk2 complex (Sheaff et al., 1997; Vlach et al., 1997; Montagnoli et al., 1999). Skp2, an F box protein that functions as the receptor component of an SCF ubiquitin ligase complex, binds to p27 only when Thr^{187} of this CKI is phosphorylated; such binding then results in the ubiquitylation and degradation of p27 (Carrano et al., 1999; Sutterluty et al., 1999; Tsvetkov et al., 1999). Skp2 also targets free cyclin E (not that complexed with Cdk2) for ubiquitylation (Nakayama et al., 2000). These biochemical observations are supported by genetic evidence showing that both p27 and free cyclin E accumulate to high levels in the cells of mice that lack Skp2 (Nakayama et al., 2000, 2001). The most obvious cellular phenotype of *Skp2*$^{-/-}$ mice is the presence of markedly enlarged, polyploid nuclei and multiple centrosomes, suggestive of an impairment in the mechanism that prevents endoreplication, in which the genomic DNA content of a cell is increased without cell division. In addition to p27 and free cyclin E, several other substrates have been proposed for Skp2. However, some of these potential substrates were found not to accumulate in cells from *Skp2*$^{-/-}$ mice, suggesting either that they are not bona fide Skp2 substrates or that functional redundancy allows for their ubiquitylation in the absence of Skp2.

Skp2 is almost undetectable or expressed at a low level in G_0 and early to mid-G_1 phase. It begins to accumulate during late G_1 phase, and its abundance is maximal during S and G_2 phases (Hara et al., 2001). The onset of Skp2 expression is unequivocally later than that of the degradation of p27 apparent at G_0-G_1. Moreover, p27 is exported from the nucleus to the cytoplasm at G_0-G_1 (Rodier et al., 2001; Ishida et al., 2002; Connor et al., 2003), whereas Skp2 is restricted to the nucleus (Miura et al., 1999). The discrepancies between the temporal and spatial patterns of p27 expression and those of Skp2 expression suggest the existence of an Skp2-independent pathway for the degradation of p27 at the G_0-G_1 transition. Indeed, the downregulation of p27 at G_0-G_1 occurs normally in *Skp2*$^{-/-}$ cells, but that in S and G_2 phases is impaired (Hara et al., 2001). These findings suggest that the major role of Skp2 might be to reduce the concentration of p27 during S and G_2 phases rather than at late G_1 phase.

To determine whether the accumulation of p27 is essential for the polyploidy and centrosome overduplication in *Skp2*$^{-/-}$ cells, we generated double mutant mice that lack both Skp2 and p27 genes. We now show that, although cyclin E accumulates in the cells of *Skp2*$^{-/-}$ *p27*$^{-/-}$ mice, the markedly enlarged, polyploid

*Correspondence: nakayak1@bioreg.kyushu-u.ac.jp
[5]These authors contributed equally to this work.

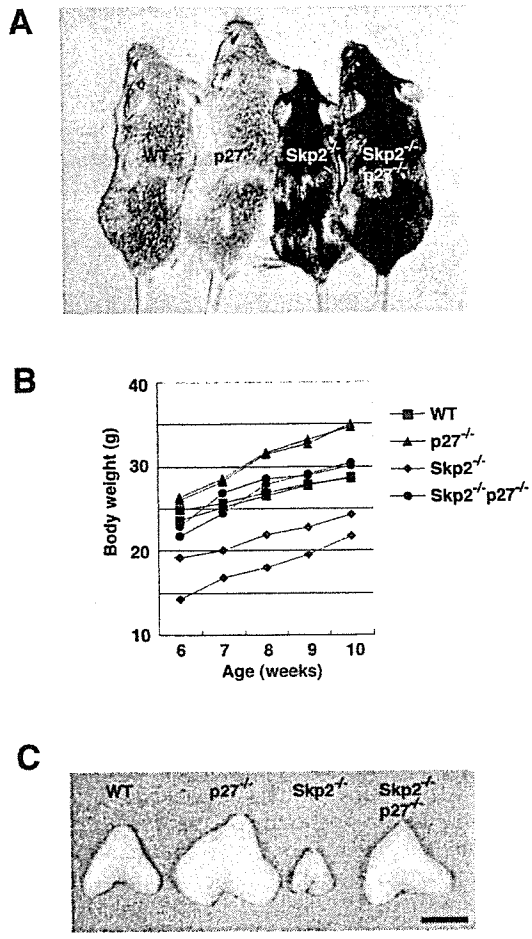

Figure 1. Body and Thymus Size in *Skp2*$^{-/-}$ *p27*$^{-/-}$ Mice

(A) Representative male wild-type (WT), *p27*$^{-/-}$, *Skp2*$^{-/-}$, and *Skp2*$^{-/-}$ *p27*$^{-/-}$ littermates at 8 weeks of age.

(B) Representative growth curves for male wild-type, *p27*$^{-/-}$, *Skp2*$^{-/-}$, and *Skp2*$^{-/-}$ *p27*$^{-/-}$ mice. Similar differences in body weight were apparent for female mice of the various genotypes (data not shown).

(C) Gross appearance of the thymus of male wild-type, *p27*$^{-/-}$, *Skp2*$^{-/-}$, and *Skp2*$^{-/-}$ *p27*$^{-/-}$ littermates at 8 weeks of age. Scale bar, 5 mm.

nuclei and multiple centrosomes associated with Skp2 deficiency are not evident in the double mutant mice. These data suggest that accumulation of p27 is primarily responsible for this cellular phenotype of *Skp2*$^{-/-}$ mice. We also demonstrate that the aberrant increase in p27 expression in *Skp2*$^{-/-}$ cells results in inhibition of the kinase activity of Cdc2 and a consequent block of entry into M phase. Our results thus indicate that Skp2 plays a crucial role in regulation of G_2-M progression by contributing to the ubiquitylation-mediated proteolysis of p27.

Results

Generation of Mice Lacking Both Skp2 and p27

To generate mice lacking Skp2 and p27, we crossed *Skp2*$^{+/-}$ *p27*$^{+/-}$ animals. As we previously described (Nakayama et al., 1996, 2000), the body size of *p27*$^{-/-}$ animals is larger and that of *Skp2*$^{-/-}$ mice is smaller than that of wild-type controls (Figures 1A and 1B). The body size of the *Skp2*$^{-/-}$ *p27*$^{-/-}$ double mutant was slightly larger than that of wild-type controls. We also examined the size of the thymus, which is one of the most affected organs in *Skp2*$^{-/-}$ or *p27*$^{-/-}$ mice; it is hyperplastic in *p27*$^{-/-}$ mice and atrophic in *Skp2*$^{-/-}$ mice (Figure 1C). As with body size, the thymus of *Skp2*$^{-/-}$ *p27*$^{-/-}$ mice was slightly larger than that of wild-type animals. In general, the *Skp2*$^{-/-}$ *p27*$^{-/-}$ mice appeared similar to *p27*$^{-/-}$ mice and exhibited phenotypes opposite to those of *Skp2*$^{-/-}$ mice. The observation that the *Skp2*$^{-/-}$ *p27*$^{-/-}$ double mutant appears similar but not identical to the *p27*$^{-/-}$ single mutant constitutes genetic evidence for the notion that, although p27 is the main target of Skp2, Skp2 may also mediate the ubiquitylation of other substrates.

Absence of Overreplication Phenotype in *Skp2*$^{-/-}$ *p27*$^{-/-}$ Mice

The most obvious cellular phenotype of *Skp2*$^{-/-}$ mice is the presence of markedly enlarged, polyploid nuclei and multiple centrosomes (Nakayama et al., 2000). To determine whether these characteristics are dependent on p27 accumulation, we examined liver, kidney, and lung cells of wild-type, *Skp2*$^{-/-}$, *p27*$^{-/-}$, and *Skp2*$^{-/-}$ *p27*$^{-/-}$ mice (Figures 2A–2L). As previously described, the nuclei of hepatocytes, renal tubule cells, and bronchiolar epithelial cells of *Skp2*$^{-/-}$ mice were substantially larger than those of the corresponding cells in wild-type littermates. Such nuclear enlargement was not apparent in the cells of *p27*$^{-/-}$ or *Skp2*$^{-/-}$ *p27*$^{-/-}$ mice. Flow cytometry also revealed that the DNA content of hepatocytes from *Skp2*$^{-/-}$ mice ranged from 2C to 16C, whereas that of most hepatocytes from wild-type or *p27*$^{-/-}$ animals was 2C or 4C (Figures 2M–2O). The percentage of polyploid cells in *Skp2*$^{-/-}$ *p27*$^{-/-}$ mice was greatly reduced compared with that in *Skp2*$^{-/-}$ mice, although the double mutant did exhibit a small increase in the number of 8C cells relative to that in wild-type animals (Figure 2P).

With the use of fluorescence microscopy, we also examined the nuclear size (as revealed by Hoechst 33258 staining) and centrosome number (as revealed by immunostaining with antibodies to pericentrin) of cultured mouse embryonic fibroblasts (MEFs) derived from the various mice. As with liver, kidney, and lung cells, MEFs derived from *Skp2*$^{-/-}$ mice exhibited a markedly enlarged nucleus, whereas the nuclear size of *Skp2*$^{-/-}$ *p27*$^{-/-}$ MEFs was similar to that of wild-type MEFs (Figures 2Q–2S). The number of centrosomes, which was increased in the *Skp2*$^{-/-}$ MEFs, also appeared normal in the *Skp2*$^{-/-}$ *p27*$^{-/-}$ cells (Figures 2T–2W). These observations indicate that the cellular phenotype of *Skp2*$^{-/-}$ mice is dependent on the presence of an intact p27 gene.

Mice lacking p27 manifest multiple organ hyperplasia, retinal dysplasia, and pituitary tumors (Fero et al., 1996; Kiyokawa et al., 1996; Nakayama et al., 1996). The most hyperplastic organs in these animals are the thymus, testis, ovary, adrenal medulla, and intermediate lobe of the pituitary gland. Histopathologic examination revealed that the adrenal medulla of *Skp2*$^{-/-}$ *p27*$^{-/-}$ mice is as hyperplastic as is that of *p27*$^{-/-}$ mice, whereas that of *Skp2*$^{-/-}$ mice appeared hypoplastic (Figures 3A–3D). Similarly, the intermediate lobe of the pituitary, a vestigial structure in adult humans, was hyperplastic in both

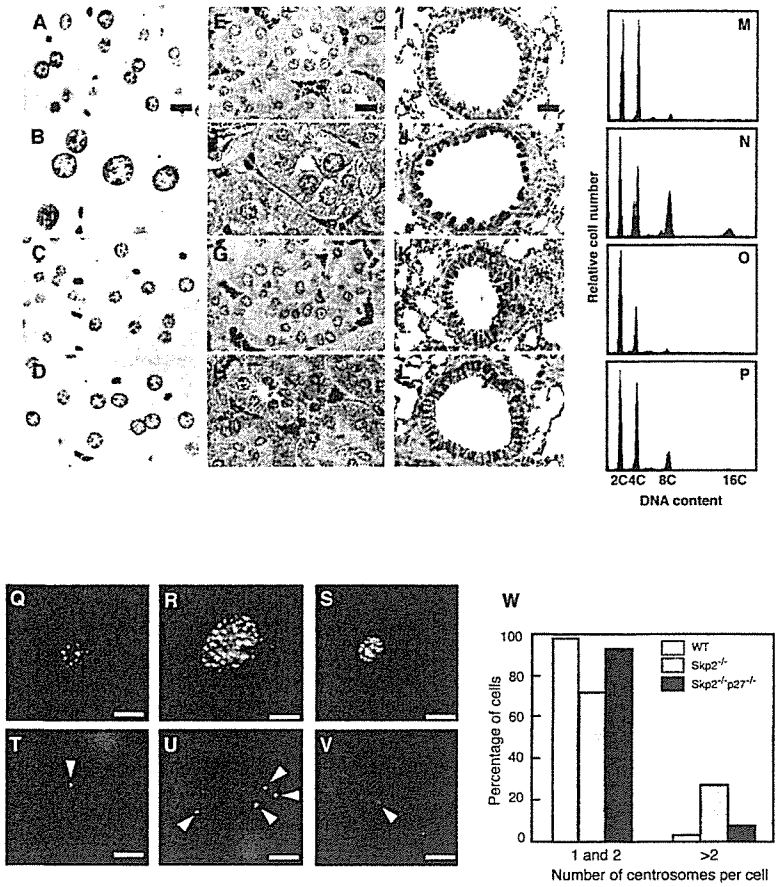

Figure 2. Absence of Nuclear Enlargement and Polyploidy in *Skp2*$^{-/-}$ *p27*$^{-/-}$ Mice

(A–L) Histological analysis of liver (A–D), renal tubules (E–H), and bronchioles (I–L) of adult wild-type (A, E, and I), *Skp2*$^{-/-}$ (B, F, and J), *p27*$^{-/-}$ (C, G, and K), and *Skp2*$^{-/-}$ *p27*$^{-/-}$ (D, H, and L) mice. Sections were stained with Feulgen solution (A–D) or with hematoxylin-eosin (E–L). Scale bars, 25 μm.

(M–P) Flow cytometric analysis of the DNA content of hepatocytes from wild-type (M), *Skp2*$^{-/-}$ (N), *p27*$^{-/-}$ (O), and *Skp2*$^{-/-}$ *p27*$^{-/-}$ (P) mice.

(Q–W) Normal nuclear size and centrosome number of *Skp2*$^{-/-}$ *p27*$^{-/-}$ cells. MEFs derived from wild-type (Q and T), *Skp2*$^{-/-}$ (R and U), and *Skp2*$^{-/-}$ *p27*$^{-/-}$ (S and V) embryos were stained either with both antibodies to β-tubulin and Hoechst 33258 (Q–S) or with antibodies to pericentrin alone (T–V). β-tubulin and pericentrin immune complexes are represented by red and green staining, respectively. Centrosomes are indicated by arrowheads. Blue staining represents Hoechst 33258 labeling of nuclear DNA. Scale bars, 10 μm. The percentages of MEFs either with one or two or with more than two centrosomes were determined by analysis of 400 cells per genotype (W).

p27$^{-/-}$ and *Skp2*$^{-/-}$ *p27*$^{-/-}$ mice (Figures 3E–3H). The intermediate lobe of these animals contained a large number of atypical cells; both *p27*$^{-/-}$ and *Skp2*$^{-/-}$ *p27*$^{-/-}$ mice were thus diagnosed with benign pituitary adenoma. Furthermore, histopathologic examination of the retina of *Skp2*$^{-/-}$ *p27*$^{-/-}$ mice revealed a marked disorganization of the cellular layers in the neural retina, similar to that apparent in *p27*$^{-/-}$ mice (Figures 3I–3L). These observations demonstrate that *Skp2*$^{-/-}$ *p27*$^{-/-}$ double mutant mice preserve the phenotypes of *p27*$^{-/-}$ mice. They therefore constitute genetic evidence in support of the notion that Skp2 is an upstream regulator of p27, although slight differences between *p27*$^{-/-}$ and *Skp2*$^{-/-}$ *p27*$^{-/-}$ mice may reflect other possible functions of Skp2.

Impaired Entry into M Phase in *Skp2*$^{-/-}$ Cells

We hypothesized that the nuclear enlargement, polyploidy, and centrosome overduplication apparent in *Skp2*$^{-/-}$ cells result from reentry of the cells into S phase without passage through M phase. To test this hypothesis, we orally administered the female hormone estriol, which transiently stimulates hepatocyte proliferation (Fujii et al., 1985), to adult wild-type, *Skp2*$^{-/-}$, *p27*$^{-/-}$, and *Skp2*$^{-/-}$ *p27*$^{-/-}$ mice. The giant cells observed in the liver of *Skp2*$^{-/-}$ mice were shown to have entered S phase by their incorporation of 5-bromo-2′-deoxyuridine (BrdU) that was injected intraperitoneally (Figures 4A and 4B). Monitoring of the time-dependent increase in the percentage of cells in S phase revealed no marked difference between wild-type and *Skp2*$^{-/-}$ mice (Figure 4C). Mitotic cells in the liver were evaluated by hematoxylin-eosin staining (data not shown) and immunostaining with antibodies to phosphorylated histone H3 (Figures 4D–4G), which is a marker for cells in M phase. In wild-type mice, cells containing phosphorylated histone H3 were apparent and peaked in number 5 days after estriol administration (Figure 4H). In contrast, no cells that reacted with the antibodies to the phosphorylated histone were detected at any time after estriol treatment in *Skp2*$^{-/-}$ mice. This lack of M phase induction in response to estriol appeared to be attributable to p27 accumulation, given that the liver of *Skp2*$^{-/-}$ *p27*$^{-/-}$ mice responded in a manner similar to that of the liver of wild-type mice (Figure 4G). These results thus suggested that *Skp2*$^{-/-}$ cells are able to enter S phase but not M phase, a characteristic of endoreplication, although a mitotic defect could also account for this abnormality. They also indicate that the inability of *Skp2*$^{-/-}$ cells to enter M phase is due to the abnormal accumulation of p27.

Impairment of Mitotic Entry Induced by a Reduction in Cdc2 Activity

In fission yeast, overexpression of the CKI Rum1 inhibits mitotic cyclin-Cdc2 activity and thereby prevents mitosis (Correa-Bordes and Nurse, 1995). Moreover, a high activity of the mitotic cyclin-Cdc2 complex prevents chromosome replication (Stern and Nurse, 1996). These observations led us to test the hypothesis that accumulation of the CKI p27 during G_2 phase inhibits mitotic cyclin-Cdc2 activity in mammalian *Skp2*$^{-/-}$ cells.

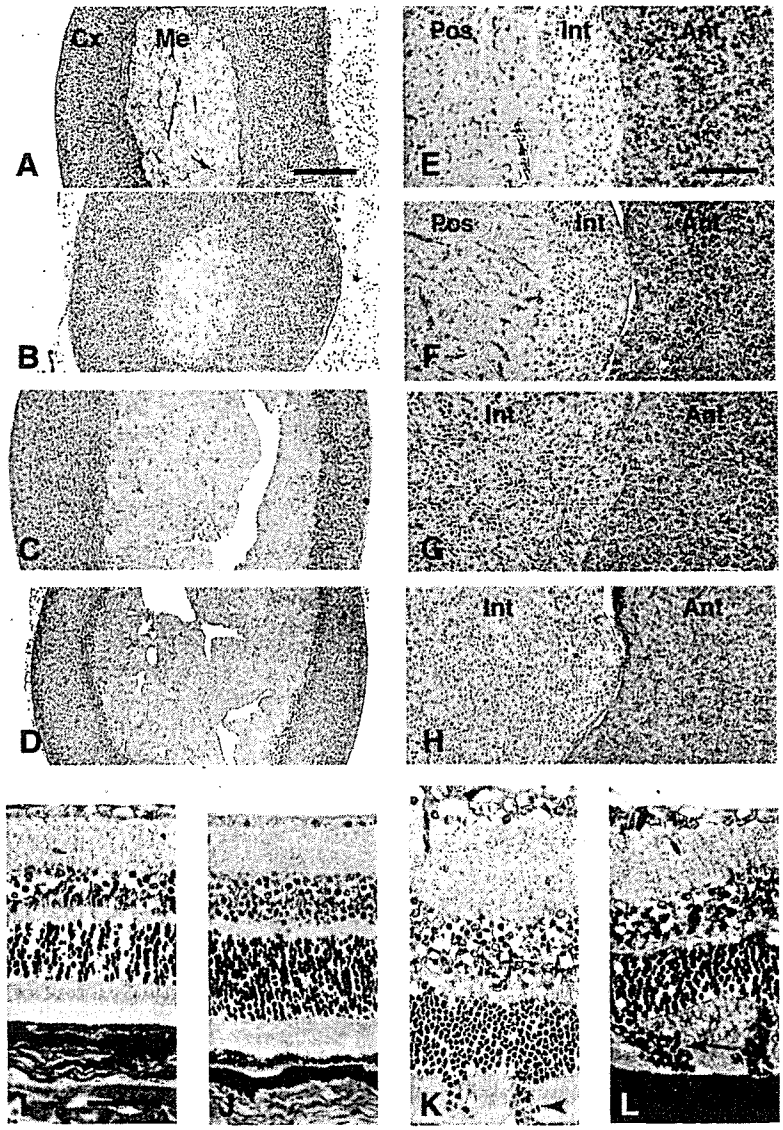

Figure 3. Organ Hyperplasia in *Skp2*$^{-/-}$ *p27*$^{-/-}$ Mice

Histological sections of the adrenal gland (A–D), pituitary gland (E–H), and retina (I–L) of wild-type (A, E, and I), *Skp2*$^{-/-}$ (B, F, and J), *p27*$^{-/-}$ (C, G, and K), and *Skp2*$^{-/-}$ *p27*$^{-/-}$ (D, H, and L) mice are shown. The paraffin-embedded sections were stained with hematoxylin-eosin. Abbreviations: Cx, cortex; Me, medulla; Ant, anterior lobe; Int, intermediate lobe; Pos, posterior lobe. Arrowheads in (K) and (L) indicate the outer granular layer invading the layer of rods and cones beyond the outer limiting membrane of the retina. Scale bars: 400 μm (A–D), 100 μm (E–H), and 25 μm (I–L).

We compared the abundance (Figure 5A) and kinase activities (Figure 5B) of various cell cycle regulators in MEFs derived from wild-type, *Skp2*$^{-/-}$, *p27*$^{-/-}$, and *Skp2*$^{-/-}$ *p27*$^{-/-}$ mice. There were no marked differences in the amounts of cyclin A, cyclin B, Cdk2, or Cdc2 or in the kinase activity associated with Cdk2 among the four types of cells. In contrast to lymphocytes, which express p27 but not p57 (Nagahama et al., 2001), and in which the loss of p27 results in a marked increase in the kinase activity of Cdk2 (Nakayama et al., 1996), *p27*$^{-/-}$ MEFs did not exhibit an increase in such activity, probably because of the presence of p57. Cyclin A-, cyclin B-, or Cdc2-associated kinase activity was substantially reduced in *Skp2*$^{-/-}$ cells compared with that in MEFs of the other three genotypes, however. The observation that *Skp2*$^{-/-}$ *p27*$^{-/-}$ MEFs differed from *Skp2*$^{-/-}$ cells in this regard suggests that accumulation of p27 is responsible for the low kinase activity of cyclin A-Cdc2 or cyclin B-Cdc2 in *Skp2*$^{-/-}$ cells. Cyclin E-associated kinase activity was not increased, even though the abundance of cyclin E was increased, in the *Skp2*$^{-/-}$ cells, suggesting that the accumulated p27 antagonized the kinase activity. Consistent with this notion, the activity of cyclin E-associated kinase activity was increased in *Skp2*$^{-/-}$ *p27*$^{-/-}$ MEFs.

We found that p27 associated with Cdc2, although to only a small extent, in wild-type MEFs (Figure 5C). The amount of Cdc2 bound to endogenous p27 was markedly increased in *Skp2*$^{-/-}$ cells, however. The phosphorylation status of tyrosine-15 and threonine-161 of Cdc2 was similar among the four genotypes of MEFs (Supplemental Figure S1 at http://www.developmentalcell.com/cgi/content/full/6/5/661/DC1), excluding the possibility that the loss of Skp2 or accumulation of p27 affects other molecules that regulate Cdc2 activity directly. The amount of Cdk2 associated with p27 was also increased in *Skp2*$^{-/-}$ cells (Figure 5C). In contrast, the amount of Cdk4 associated with p27 was not affected by the loss of Skp2, which might be explained if the amount of Cdk4 is limited and most of it is bound to p27 even in wild-type cells; the excess p27 that overflows from the Cdk4-bound pool would then be available to bind to Cdk2 or

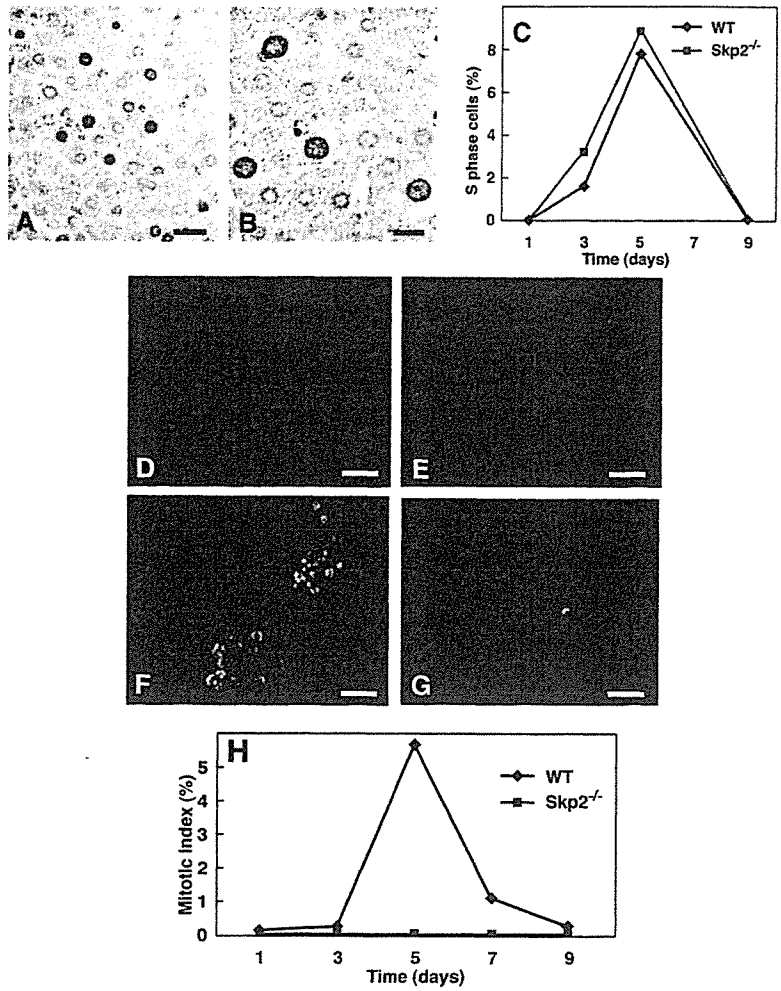

Figure 4. Defective Entry into M Phase of Hepatocytes Exposed to Mitogenic Stimulation in Adult *Skp2*$^{-/-}$ Mice

Adult mice were subjected to a single oral administration of estriol and daily intraperitoneal injection of BrdU. They were killed at various times after estriol administration and sections of the liver were processed for immunostaining.

(A and B) Liver sections prepared from wild-type (A) and *Skp2*$^{-/-}$ (B) mice 5 days after administration of estriol were subjected to immunostaining with antibodies to BrdU (brown).

(C) The percentage of liver cells that stained with the antibodies to BrdU was determined for wild-type and *Skp2*$^{-/-}$ mice at the indicated times after administration of estriol.

(D–G) Liver sections prepared from wild-type (D), *Skp2*$^{-/-}$ (E), *p27*$^{-/-}$ (F), and *Skp2*$^{-/-}$ *p27*$^{-/-}$ (G) mice 5 days after estriol administration were stained with antibodies to phosphorylated histone H3 (red) and Hoechst 33258 (blue).

(H) The percentage of liver cells that stained with the antibodies to phosphorylated histone H3 (mitotic index) was determined for wild-type and *Skp2*$^{-/-}$ mice at the indicated times after administration of estriol.

Data in (C) and (H) are from representative animals. Scale bars: 50 μm (A and B) and 25 μm (D–G).

Cdc2 in *Skp2*$^{-/-}$ MEFs. Immunodepletion of p27 also reduced the amounts of Cdc2 and Cdk2 in *Skp2*$^{-/-}$ cell lysates (data now shown), confirming that a substantial proportion of Cdc2 and Cdk2 is bound to endogenous p27. We also found that FLAG epitope-tagged exogenous p27 interacted with endogenous cyclin A, cyclin B, Cdk2, and Cdc2 as well as inhibited the associated kinase activities in COS-7 cells (Figure 5D). Mass spectrometric analysis of immunoprecipitates prepared from HEK293T cells expressing FLAG-tagged p27 with antibodies to FLAG showed that p27 is complexed with cyclin A2, cyclin B1, cyclin B2, cyclin E1, cyclin E2, Cdc2, Cdk2, Cdk4, and Cdk5 (data not shown).

We next examined whether the observed decrease in the kinase activity of Cdc2 is sufficient to explain the overreplication phenotype of *Skp2*$^{-/-}$ cells. We first treated wild-type MEFs with a potent Cdc2 inhibitor, butyrolactone I (Kitagawa et al., 1993). Exposure of the wild-type MEFs to butyrolactone I resulted in nuclear enlargement and centrosome multiplication (Figures 6A and 6B), characteristics similar to those of *Skp2*$^{-/-}$ MEFs. Flow cytometric analysis revealed that the DNA content of the butyrolactone I-treated cells increased in multiples of 2C (Figure 6C), a characteristic of endoreplication, rather than in a continuous manner, as would be consistent with DNA rereplication. Cell size was also increased by treatment with butyrolactone I (Figure 6D). Given that this compound may affect other types of Cdk, we also examined FT210 cells, which express a temperature-sensitive mutant of Cdc2 (Th'ng et al., 1990). FM210 cells cultured at the restrictive temperature (39°C) exhibited huge nuclei and multiple centrosomes (Figure 6H); neither FM210 cells cultured at the permissive temperature (32°C) (Figure 6G) nor the parental cell line, FM3A, cultured at either temperature (Figures 6E and 6F) exhibited this phenotype. Flow cytometric analysis revealed that FT210 cells cultured at the restrictive temperature, but not those cultured at the permissive temperature, appeared to be arrested at the G_2-M boundary (Figure 6I) with an increase in cell size (Figure 6J). These data thus indicate that a reduction in the kinase activity of Cdc2 results in G_2-M arrest associated with nuclear enlargement and centrosome overduplication in mammalian cells. In *Skp2*$^{-/-}$ mice, the accumulation of p27 due to the lack of its ubiquitylation-mediated proteolysis likely results in such a decrease in Cdc2 activity.

Accumulation of Cyclin E in *Skp2*$^{-/-}$ *p27*$^{-/-}$ Mice

Given that p27 is an inhibitor of the kinase activity of cyclin E-Cdk2 and that the phosphorylation of cyclin E that triggers its degradation is thought to be mediated,